Cell

Exome Capture Reveals *ZNF423* and *CEP164* Mutations, Linking Renal Ciliopathies to DNA Damage Response Signaling

Moumita Chaki,[1,39] Rannar Airik,[1,39] Amiya K. Ghosh,[1] Rachel H. Giles,[3] Rui Chen,[4] Gisela G. Slaats,[3] Hui Wang,[4] Toby W. Hurd,[1] Weibin Zhou,[1] Andrew Cluckey,[1] Heon Yung Gee,[1] Gokul Ramaswami,[1] Chen-Jei Hong,[6] Bruce A. Hamilton,[6] Igor Červenka,[7] Ranjani Sri Ganji,[7] Vitezslav Bryja,[7,8] Heleen H. Arts,[9] Jeroen van Reeuwijk,[9] Machteld M. Oud,[9] Stef J.F. Letteboer,[9] Ronald Roepman,[9] Hervé Husson,[10] Oxana Ibraghimov-Beskrovnaya,[10] Takayuki Yasunaga,[11] Gerd Walz,[11] Lorraine Eley,[12] John A. Sayer,[12] Bernhard Schermer,[13,14,16] Max C. Liebau,[13,15] Thomas Benzing,[13,14,16] Stephanie Le Corre,[19] Iain Drummond,[19] Sabine Janssen,[1] Susan J. Allen,[1] Sivakumar Natarajan,[1] John F. O'Toole,[20] Massimo Attanasio,[21] Sophie Saunier,[22] Corinne Antignac,[22] Robert K. Koenekoop,[23] Huanan Ren,[23] Irma Lopez,[23] Ahmet Nayir,[24] Corinne Stoetzel,[25] Helene Dollfus,[25] Rustin Massoudi,[26] Joseph G. Gleeson,[26] Sharon P. Andreoli,[27] Dan G. Doherty,[28] Anna Lindstrad,[29] Christelle Golzio,[29] Nicholas Katsanis,[29] Lars Pape,[30] Emad B. Abboud,[31] Ali A. Al-Rajhi,[31] Richard A. Lewis,[5] Heymut Omran,[32] Eva Y.-H.P. Lee,[33] Shaohui Wang,[33] JoAnn M. Sekiguchi,[2] Rudel Saunders,[2] Colin A. Johnson,[34] Elizabeth Garner,[35] Katja Vanselow,[36] Jens S. Andersen,[36] Joseph Shlomai,[18] Gudrun Nurnberg,[14,17] Peter Nurnberg,[14,17] Shawn Levy,[37] Agata Smogorzewska,[35] Edgar A. Otto,[1] and Friedhelm Hildebrandt[1,2,38,*]

[1]Department of Pediatrics and Communicable Diseases
[2]Department of Human Genetics
University of Michigan, Ann Arbor, MI 48109, USA
[3]Department of Nephrology and Hypertension, University Medical Center, Utrecht, The Netherlands
[4]HGSC Department of Molecular and Human Genetics
[5]Department of Ophthalmology
Baylor College of Medicine, Houston, TX, USA
[6]Department of Medicine, Division of Medical Genetics, Department of Cellular and Molecular Medicine, and Institute for Genomic Medicine, George Palade Laboratories, Room 256, UCSD School of Medicine, 9500 Gilman Drive, San Diego, CA 92093, USA
[7]Institute of Experimental Biology, Faculty of Science, Masaryk University, 61137 Brno, Czech Republic
[8]Department of Cytokinetics, Institute of Biophysics, Academy of Sciences of the Czech Republic 61265 Brno, Czech Republic
[9]Department of Human Genetics, Nijmegen Centre for Molecular Life Sciences and Institute for Genetic and Metabolic Disease, Radboud University Nijmegen Medical Centre, 6525 GA, Nijmegen, The Netherlands
[10]Genzyme Corporation, Cell Biology, Framingham, MA 01701, USA
[11]Renal Division, University Freiburg Medical Center, 7900 Freiburg, Germany
[12]Institute of Genetic Medicine, Newcastle University, Newcastle upon Tyne, NE1 3BZ, UK
[13]Department II of Internal Medicine and Center for Molecular Medicine
[14]Cologne Excellence Cluster on Cellular Stress Responses in Aging-Associated Diseases
[15]Department of Pediatrics and Adolescent Medicine
[16]Systems Biology of Aging
[17]Cologne Center for Genomics and for Molecular Medicine
University of Cologne, 50937 Cologne, Germany
[18]Department of Microbiology and Molecular Genetics, The Institute for Medical Research Israel-Canada (IMRIC), Faculty of Medicine, The Hebrew University-Hadassah Medical School, Jerusalem, 91120 Israel
[19]Nephrology Division, Massachusetts General Hospital and Department of Genetics, Harvard Medical School, Charlestown, MA 02129, USA
[20]Division of Nephrology, Department of Internal Medicine, MetroHealth Medical Center, and Case Western Reserve University School of Medicine, Cleveland, OH 44109-1998, USA
[21]Department of Internal Medicine and Eugene McDermott Center for Growth and Development, University of Texas Southwestern Medical Center, Dallas TX 75390, USA
[22]Inserm U983, Paris Descartes University, Hôpital Necker-Enfants Malades, Assistance Publique-Hôpitaux de Paris, Paris, France
[23]McGill Ocular Genetics Laboratory, Montreal Children's Hospital, McGill University Health Centre, Montreal, H3H 1P3, Canada
[24]Department of Pediatric Nephrology, Faculty of Medicine, University of Istanbul, Istanbul, Turkey
[25]Laboratoire de Génétique Médicale EA3949, Equipe AVENIR-Inserm, Faculté de Médecine, Université de Strasbourg, 11 rue Humann, 67000 Strasbourg, France
[26]Howard Hughes Medical Institute, Department of Pediatrics, University of California, San Diego, La Jolla, CA 92093, USA
[27]Department of Pediatrics, James Whitcomb Riley Hospital for Children, Indiana University Medical Center, Indianapolis, IN 46202, USA
[28]Division of Genetic Medicine, Department of Pediatrics, University of Washington, Center for Integrative Brain Research, Seattle Children's Hospital, Seattle, WA, 98101 USA
[29]Center for Human Disease Modeling, Duke University Medical Center, Durham, NC 27710, USA
[30]Department of Pediatric Nephrology, Hannover Medical School, Hannover 30625, Germany
[31]King Khaled Eye Specialist Hospital, Riyadh 11462, Kingdom of Saudi Arabia

[32]Klinik und Poliklinik für Kinder- und Jugendmedizin, Allgemeine Pädiatrie, Universitätsklinikum Münster, Münster 48149, Germany
[33]University of California Irvine, Department of Biological Chemistry, Irvine, CA 92697, USA
[34]Leeds Institute of Molecular Medicine, St James's University Hospital, Leeds, LS9 7TF, UK
[35]Laboratory of Genome Maintenance, The Rockefeller University, New York, NY 10065, USA
[36]Department of Biochemistry and Molecular Biology, University of Southern Denmark, DK-5230, Odense, Denmark
[37]HudsonAlpha Institute for Biotechnology, 601 Genome Way, Huntsville, AL 35806, USA
[38]Howard Hughes Medical Institute, Chevy Chase, MD 20815, USA
[39]These authors contributed equally to this work
*Correspondence: fhilde@umich.edu
http://dx.doi.org/10.1016/j.cell.2012.06.028

SUMMARY

Nephronophthisis-related ciliopathies (NPHP-RC) are degenerative recessive diseases that affect kidney, retina, and brain. Genetic defects in *NPHP* gene products that localize to cilia and centrosomes defined them as "ciliopathies." However, disease mechanisms remain poorly understood. Here, we identify by whole-exome resequencing, mutations of *MRE11*, *ZNF423*, and *CEP164* as causing NPHP-RC. All three genes function within the DNA damage response (DDR) pathway. We demonstrate that, upon induced DNA damage, the NPHP-RC proteins ZNF423, CEP164, and NPHP10 colocalize to nuclear foci positive for TIP60, known to activate ATM at sites of DNA damage. We show that knockdown of *CEP164* or *ZNF423* causes sensitivity to DNA damaging agents and that *cep164* knockdown in zebrafish results in dysregulated DDR and an NPHP-RC phenotype. Our findings link degenerative diseases of the kidney and retina, disorders of increasing prevalence, to mechanisms of DDR.

INTRODUCTION

Nephronophthisis (NPHP) is a recessive cystic kidney disease that represents the most frequent genetic cause of end-stage kidney disease in the first three decades of life. NPHP-related ciliopathies (NPHP-RC) are single-gene recessive disorders that affect kidney, retina, brain, and liver by prenatal-onset dysplasia or by organ degeneration and fibrosis in early adulthood. Identification of recessive mutations in more than ten different genes (*NPHP1-NPHP*13) revealed that their gene products share localization at the primary cilia-centrosomes complex and mitotic spindle poles in a cell-cycle-dependent manner, characterizing them as retinal-renal "ciliopathies" (Ansley et al., 2003; Hildebrandt et al., 2011). Multiple signaling pathways downstream of cilia have been implicated in the disease mechanisms of NPHP-RC, including Wnt signaling (Germino, 2005; Simons et al., 2005) and Shh signaling (Huangfu and Anderson, 2005; Huangfu et al., 2003). However, despite convergence of ciliopathy pathogenesis at cilia and centrosomes it remains largely unknown what signaling pathways downstream of cilia and centrosome function operate in the disease mechanisms that generate the NPHP-RC phenotypes.

Centrosomal proteins have been recently implicated in DNA damage response (DDR). Both pericentrin (PCNT), a core centrosomal protein (Doxsey et al., 1994), as well as CEP152, encoding a centrosomal protein required for centriolar duplication (Blachon et al., 2008), are defective in Seckel syndrome, an autosomal-recessive disorder characterized by dwarfism, microcephaly, and mental retardation (Griffith et al., 2008; Kalay et al., 2011; Rauch et al., 2008). *PCNT*- and *CEP152* mutant cells are also defective in ATR-dependent DDR signaling, consistent with the fact that the first mutation identified in Seckel syndrome was in ataxia-telangiectasia mutated and RAD3-related (ATR), a key phosphoinositide 3-kinase-related protein kinase involved in DDR signaling (O'Driscoll et al., 2003), but the mechanism of the signaling defect is not fully understood.

The known *NPHP* genes explain less than 50% of all cases with NPHP-RC, and many of the single-gene causes of NPHP-RC are still unknown (Otto et al., 2011). The finding that some of the recently identified genetic causes of NPHP-RC are exceedingly rare (Attanasio et al., 2007) necessitates the ability to identify novel single-gene causes of NPHP-RC in single affected families. To achieve this goal, we developed a strategy that combines homozygosity mapping (HM) with whole-exome resequencing (WER) (Otto et al., 2010). Because this approach allows identification of multiple different causes of NPHP-RC within a short time frame, it has the potential of delineating pathogenic pathways.

Using this approach, we identify here mutations in three NPHP-RC genes, *MRE11*, *ZNF423*, and *CEP164*, which together suggest involvement of a DDR signaling pathway in NPHP-RC pathogenesis.

RESULTS

Whole-Exome Resequencing Accelerates Discovery of *NPHP-RC* Genes

Identification of monogenic causes of ciliopathies is limited by their rarity (Attanasio et al., 2007), necessitating methods to identify ciliopathy-causing genes in *single* families by using WER. However, WER typically yields hundreds of variants from normal reference sequence (Ng et al., 2009), whereas only a single-gene mutation will represent the disease cause. To overcome this limitation, we here combined WER with HM (Hildebrandt et al., 2009) in sib pairs affected with NPHP-RC and performed functional analysis of the identified genes (Otto et al., 2010).

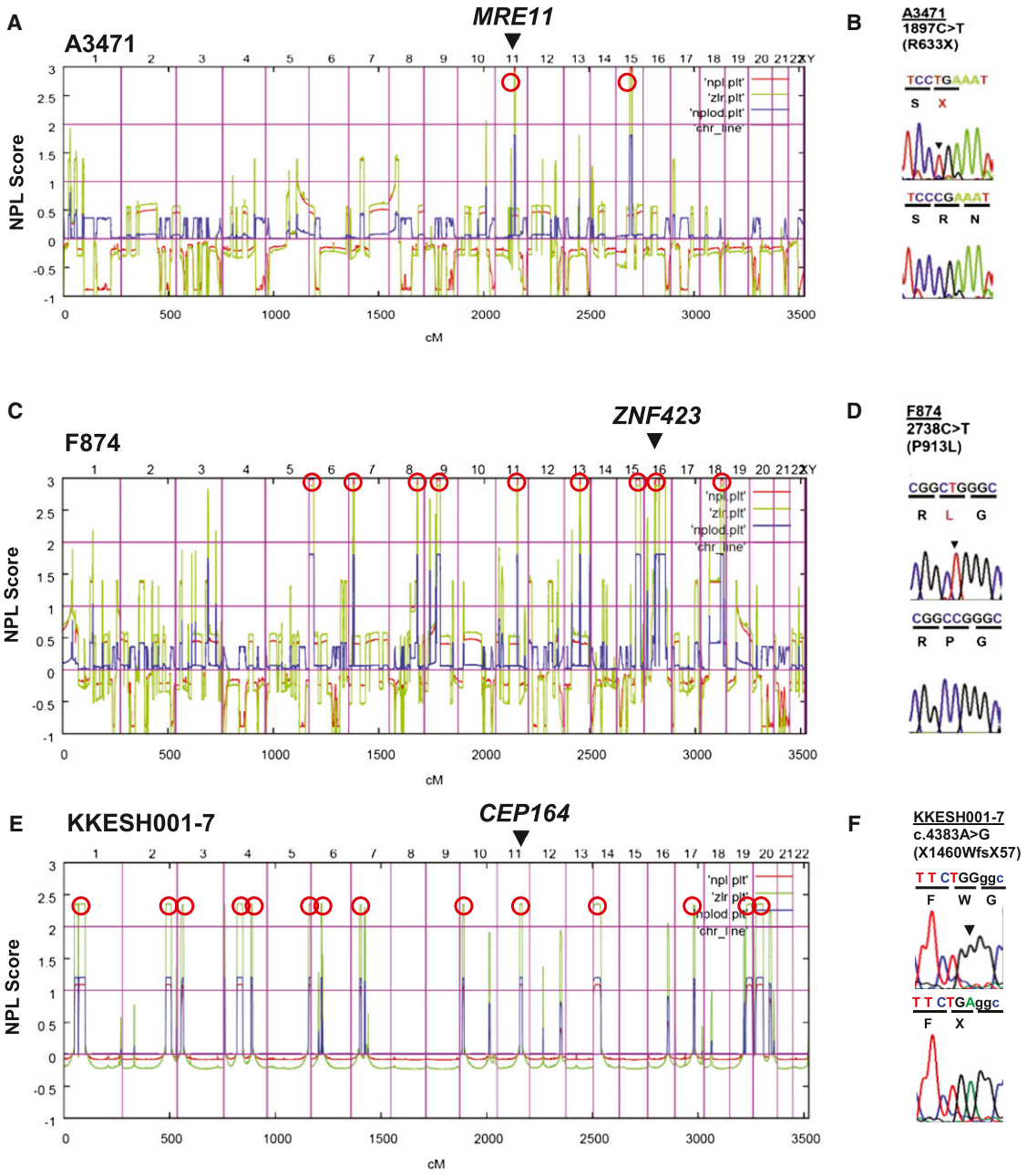

Figure 1. Identification of Recessive Mutations in *MRE11*, *ZNF423*, and *CEP164* in NPHP-RC Using HM and WER

Data regarding HM and mutations are shown for family A3471 with *MRE11* mutation (A and B), family F874 with *ZNF423* mutation (C and D), and family KKESH001 with *CEP164* mutation (E and F). (A, C, and E) Nonparametric lod scores (NPL) are plotted across the human genome in three families (A3471, F874, and KKESH001) with NPHP-RC (see also Table 1). The x axis shows SNP positions on human chromosomes concatenated from *p*-ter (left) to *q*-ter (right). Genetic distance is given in cM. Maximum NPL peaks (Hildebrandt et al., 2009) (red circles) indicate candidate regions of homozygosity by descent. The genes *MRE11*, *ZNF423*, and *CEP164* are positioned (arrow heads) within one of the maximum NPL peaks. (B, D, and F) Homozygous mutations detected in families with NPHP-RC. Family number (underlined), mutation (arrowheads), and predicted translational changes (in parenthesis) are indicated (see also Table 1). Sequence traces are shown for mutations above normal controls. (For additional mutations in other families see also Table 1 and Figure S2).

HM yielded positional candidate regions of homozygosity by descent (Hildebrandt et al., 2009) in families A3471 (two regions), F874 (nine regions), and KKESH001-7 (14 regions) (Figure 1), who had one or more features of NPHP-RC, including NPHP, retinal degeneration, liver fibrosis, or cerebellar degeneration/hypoplasia (Table 1). We then performed WER in one affected individual of each of the three NPHP-RC families (Ng et al., 2009; Otto et al., 2010). Remarkably, each of three NPHP-RC

Table 1. Mutations of *MRE11, ZNF423* and *CEP164* in families with NPHP-RC

Family	Individuals	Ethnic Origin	Nucleotide Alteration[a,b] (Hg19 Position)	Deduced Protein Change	Exon (State)	Continuous Amino Acid Sequence Conservation	Parental Consanguinity	Kidney (Age at ESKF)	Eye (Age at RD)	Other (at Age)
MRE11										
A3471	-21 and -22	Pakistani	c.1897C>T (Chr11: 94,170,372)	p.R633X	16 (hom)	N/A	Yes	No renal failure	Normal -21:	-21: CVA (MRI), ataxia, dysarthria, myoclonus; -22: CVA (MRI), ataxia
ZNF423										
F874	-21 and -22	Turkey	c.2738C>T (Chr16: 49,670,325)	p.P913L	5 (hom)	(*D. rerio*)	Yes	NPHP	ND	CVH Infantile NPHP *Situs inversus*
A106	-21 and -22	Iceland	c.1518delC (Chr16: 49,671,545)	p.P506fsX43	5 (het)	(*X. tropicalis*)	No	PKD	LCA	CVH (Joubert)
A111	-21	?	c.3829C>T (Chr16: 49,525,212)	p.H1277Y	9 (het)	(*D. rerio*)	?	PKD	RD	CVH, NPHP, perinatal breathing abnormality, tongue tumor
CEP164										
F319	-21 and -22	Turkey	c.32A>C (Chr11: 117,209,334)	p.Q11P	3 (hom)	(*Ch. Reinhardtii*)	Yes	NPHP, no Bx; -21: (8 years); -22: (8 years)	-21: RD (11yr, not yet blind); -22: no RP at 8 yrs	-21: obesity? no LF; -22: obesity? LF?
F59	-21, -22, -23	USA (Europe)	c.277C>T, (Chr11: 117,222,588) c.1573C>T (Chr11: 117,252,580)	p.R93W, p.Q525X	5 (het), 13 (het)	(*Ch. Reinhardtii*), N/A	No	NPHP, no Bx; -21: (9 years); -22: (8 years); -23: normal	-21: RD (6 years); -22: LCA (legally blind at 5 months); -23: (2 years)	-22: NY (birth), mild AI; -23: seizures[c], substantial DD, mild ID
NPH505		ND	c.1726C>T (Chr11: 117,257,920)	p.R576X	15 (hom)	N/A	Yes	NPHP, Bx (8 yr)	RD and flat ERG (not blind)	CVH, FD, bilateral PD, bronchiectasis (1 mo), abnormal LFT, obesity
KKESH001-7		Saudi	c.4383A>G (Chr11: 117,282,884)	p.X1460W extX57	33 (hom)	N/A	Yes	normal	(RD) LCA, flat ERG (blind <2 yr)	N/A

AI, aortic insufficiency; Bx, Kidney biopsy; CVH, cerebeller vermis hypoplasia; DD, developmental delay; ERG, electroretinogram; ESKF, end-stage kidney failure; FD, facial dysmorphism; het, heterozygous; hom, homozygous; ID, intellectual disability; LCA, Leber congenital amaurosis; LF, liver fibrosis; LFT, liver function tests; MRI, magnetic resonance imaging; N/A, not applicable; ND, no data; NPHP, nephronophthisis; NPHP-RC, nephronophthisis-related ciliopathies; NY, nystagmus; PD, polydactyly; RD, retinal degeneration; SS, short stature.

[a]All mutations were absent from >270 healthy control individuals and from the ESP Exome Variant Server data base, except the *CEP164* variant p.R576X (allele frequency in European Americans 1/7,019).

[b]cDNA mutation numbering is based on human reference sequences NM_014956.4 for *MRE11*, NM_015069.2 for *ZNF423*, and NP_055771 for *CEP164*, where +1 corresponds to the A of ATG start translation codon.

[c]Seizures were intractable, generalized and/or partial complex.

genes consecutively identified by this approach, *MRE11*, *ZNF423*, and *CEP164*, suggested a functional connection to the DDR pathway (Figure 1; Table 1).

A Mutation of *MRE11* in Progressive Cerebellar Degeneration Suggests Link to DDR

In family A3471, two siblings had cerebellar vermis hypoplasia (CVH), a central feature of NPHP-RC (Table 1). Homozygosity mapping yielded two candidate loci (Figure 1A). WER detected a homozygous truncation mutation (p.R633X) of *MRE11* (Figure 1B; Table 1) previously described for CVH in another Pakistani family (Stewart et al., 1999), suggesting a founder effect for this allele. MRE11 is an essential component of the ATM-Chk2 pathway of DDR (Figure S1 available online), where it recruits ATM (ataxia telangiectasia-mutated) to sites of DNA double-strand breaks (Figure S1A). Rediscovery of this *MRE11* mutation in family A3471 thus generated an unexpected link between NPHP-RC phenotype and the ATM pathway of DDR signaling (Figure S1A).

Patients with the NPHP-RC Joubert Syndrome Have Defects in ZNF423

Another link of NPHP-RC to the ATM pathway of DDR signaling emerged from HM and WER in two siblings (F874) with infantile onset NPHP, CVH, and *situs inversus* (Table 1). SNP mapping yielded nine candidate regions of homozygosity by descent (Figure 1C). We identified in both affected individuals a homozygous missense mutation (p.P913L; conserved in vertebrates) of *ZNF423* (Figure 1D). In addition, when examining 96 additional Joubert syndrome (JS) subjects, we detected two heterozygous-only mutations of *ZNF423*: p.P506fsX43 in family A106 and p.H1277Y in individual A111-21 (Table 1). Mutations of the mouse ortholog *Zfp423* cause reduced proliferation and abnormal development of midline neural progenitors resulting in a loss of the cerebellar vermis (Alcaraz et al., 2006; Cheng et al., 2007) similar to that seen in JS patients with CVH.

ZNF423 encodes a protein with 30 zinc fingers (Figure 2A). Mouse models display phenotypic variability that is subject to modifier genes, environment, and stochastic effects (Alcaraz et al., 2011; Alcaraz et al., 2006), consistent with the variable presentations of NPHP-RC patients. The homozygous mutation p.P913L, located between zinc fingers 21 and 22 (Figure 2A), most likely exerts recessive loss-of-function, analogous to the *Zfp423* mouse models.

We next examined whether the heterozygous-only mutations (Table 1) lead to loss of function via a dominant mechanism, using a proliferation assay in P19 cells (Figures 2B–2D). Mutations were engineered into a FLAG-tagged *ZNF423* cDNA and assayed by a S-phase index, defined as the proportion of transfected cells that incorporate BrdU in 1 hr, 48 hr after transfection. Simple loss-of-function alleles should not interfere with endogenous *Zfp423* activity in this assay. Indeed, overexpression of either wild-type or the homozygous p.P913L allele had no effect (Figure 2D). However, transfection with either the p.P506fsX43 frame-shifting allele, which removes the zinc fingers required for SMAD (similar to mothers against decapentaplegic) and EBF (early B cell factor) interactions, and the H1277Y substitution allele, which destroys the terminal zinc finger required for EBF interaction, reduced the mitotic index to little more than half that of cells transfected with green fluorescent protein (GFP) control vector or other alleles of *ZNF423* (Figures 2B–2D). A dominant mechanism is plausible for the two heterozygous mutations, as each is predicted to interfere selectively with a subset of interaction domains (Figure 2A). Neither subject had siblings, and DNA from parents was not available to determine whether the mutations occurred de novo.

We detected five additional putative mutations in highly conserved (including histidine knuckle) residues of *ZNF423* among JS families (Table S1). Although these mutations have not been confirmed functionally, the high incidence of predicted deleterious mutations found in patients but absent from 270 healthy control individuals, dbSNP, and 1000 Genomes Project data further support identification of *ZNF423* as a causal gene in NPHP-RC and JS.

ZNF423/OAZ was recently shown to interact with the DNA ds-damage sensor PARP1 (poly-ADP ribosyl polymerase 1) (Ku et al., 2003), which recruits MRE11 and ATM to sites of DNA damage (Figure S1A). This indirectly linked ZNF423 to the ATM pathway of DNA damage signaling (Figure S1A). We therefore tested whether *ZNF423* mutations affect interaction between ZNF423 and PARP1. Coimmunoprecipitation verified the association of ZNF423 and PARP1 in reciprocal assays (Figure 2E). More importantly, the truncating mutation P506fsX43, which we detected in a JS patient (Table 1), abrogates this interaction (Figure 2E), whereas H1277Y inhibits multimerization of ZNF423 (Figure 2E). In addition, depletion of *ZNF423* mRNA caused sensitivity to DNA damaging agents (see below).

Furthermore, we identified ZNF423 as a direct interaction partner of CEP290/NPHP6, which is mutated in NPHP-RC (Sayer et al., 2006; Valente et al., 2006). In a yeast two-hybrid screen of human fetal brain library with a *CEP290* (JAS2; amino acids 1917–2479) "bait" we found three in-frame "prey" sequences corresponding to ZNF423 (amino acids 178-406). This interaction was confirmed (Figures 2F and 2G). CEP290/NPHP6 is known to interact with the NPHP-RC protein NPHP5 (Schäfer et al., 2008) and localizes to the ciliary transition zone (Sang et al., 2011).

Mutations of *CEP164* Cause NPHP-RC

We obtained 14 candidate regions by HM in a Saudi family (KKESH001) of first-cousin parents with a child who had LCA (which can be allelic with NPHP-RC) with nystagmus, hyperopic discs, vascular attenuation, diffuse retinal pigment epithelium atrophy, and nonrecordable ERG (Table 1) (Figure 1E). Using WER we detected a homozygous point mutation in *CEP164* (*centrosomal protein 164 kDa*) that abolished the termination codon, adding 57 amino acid residues to the open reading frame (p.X1460WextX57) (Figure 1F, Table 1). The mutation was absent from 96 Saudi healthy controls and from 224 North American LCA patients who lack mutations in other known LCA genes.

We performed exon-PCR and Sanger sequencing of all 31 coding exons for one affected individual in each of 856 different NPHP-RC families (see Extended Experimental Procedures). We detected both mutated *CEP164* alleles in each of three additional families with NPHP-RC (Table 1; Figure S2). We thereby identified recessive mutations of *CEP164* as an additional cause of NPHP-RC. Because of the significant overlap of phenotypic

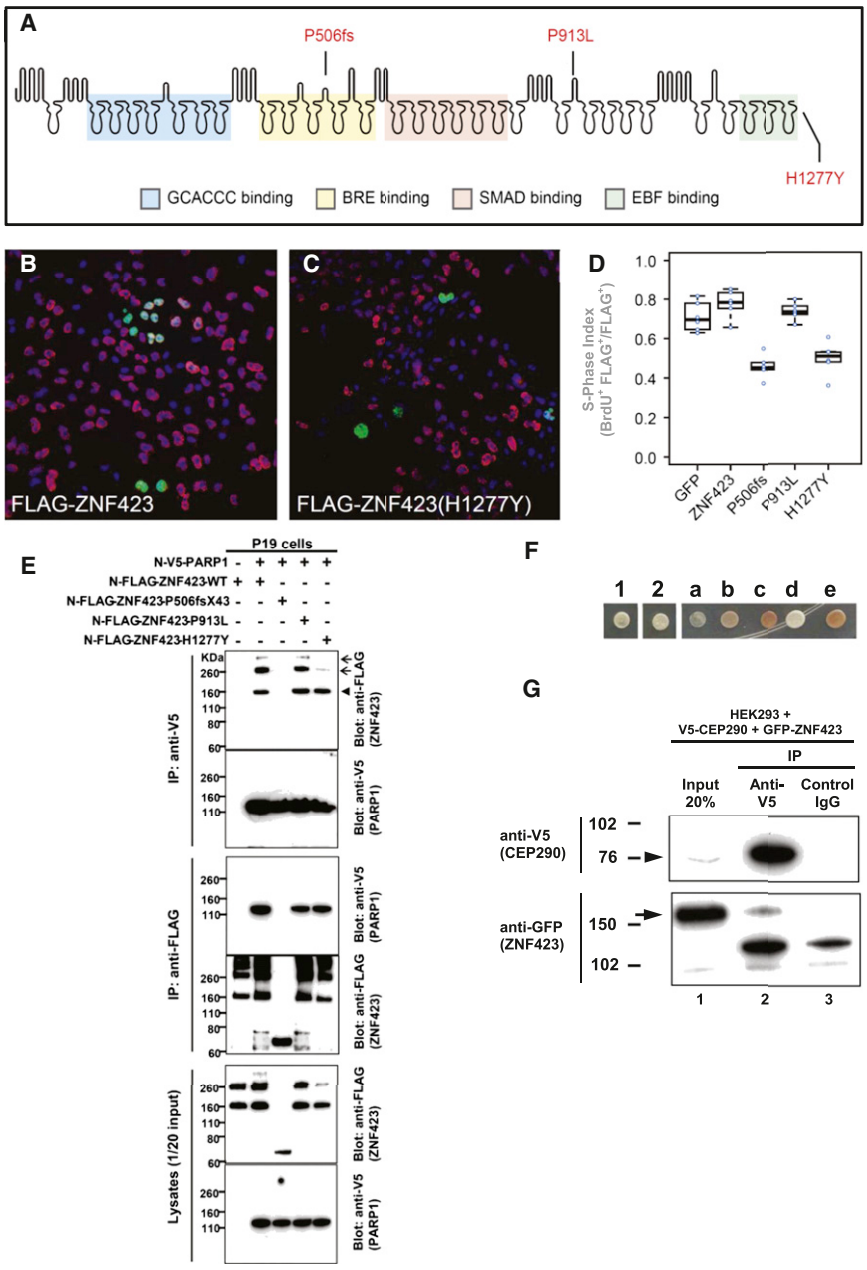

Figure 2. Two *ZNF423* Mutations Have Dominant Negative Characteristics, *ZNF423* Mutation Abrogates Interaction with PARP1, and ZNF423 Directly Interacts with the NPHP-RC Protein CEP290/NPHP6

(A) Amino acid residues altered by NPHP-RC mutations in *ZNF423* are drawn in relation to functional annotation of its 30 Zn-fingers.

(B–D) S-phase index assay (fraction of transfected cells incorporating BrdU) for P19 cells transfected with either wild-type or mutant *ZNF423*. (B) Representative field of cells transfected with wild-type *ZNF423* shows high frequency of $BrdU^+$ $FLAG^+$ double-positive cells. (C) *ZNF423–H1277Y* transfected cells exhibits fewer FLAG–positive cells and a lower proportion that are double positive. (D) S-phase index measured in duplicate transfections for each of three DNA preparations per construct. A GFP construct was used as a nonspecific control. Constructs with *P506fsX43* and *H1277Y* mutations detected in NPHP-RC show significantly reduced S-phase index ($p < 10^{-5}$, ANOVA with post-hoc Tukey honestly significant difference [HSD]).

(E) ZNF423 interacts with PARP1. P19 cells were cotransfected with expression constructs for N terminally FLAG-tagged human full-length ZNF423 and V5-tagged human full length PARP1. Comparable amounts of both proteins were present in all lysates (lower panels). Proteins were precipitated, using anti-V5 (upper panels) and anti-FLAG antibodies (middle panels), respectively. Reciprocal coIP demonstrates interaction between ZNF423 and PARP1. Note that the ZFN423 mutation P506fsX43 abrogates this interaction (arrowhead) and that mutation H1277Y diminishes ZNF423 multimerization (arrow).

(F–G) ZNF423 directly interacts with CEP290/NPHP6. (F) A human fetal brain yeast two-hybrid library screened with human CEP290/NPHP6 (JAS2; aa 1917–2479) fused to the DNA-binding domain of GAL4 (pDEST32) identified ZNF423 as a direct interaction partner of CEP290/NPHP6. The interaction was confirmed using direct yeast two-hybrid assay where 1 and 2 represent colony growth of CEP290 bait with ZNF423 prey. a–e are controls for colony growth on medium deficient in histidine, leucine and tryptophan. (G) HEK293T were cotransfected with human V5-tagged partial human *V5-CEP290* clone and GFP-tagged full-length human *ZNF423* clone. Immunoprecipitation with anti-V5 (lane 2), but not control IgG (lane 3) precipitated both the V5-tagged CEP290 (arrowhead) as well as GFP-tagged ZNF423 (arrow).

features with other forms of NPHP-RC we introduce the alias "NPHP14" for ZNF423 and "NPHP15" for the CEP164 protein.

Although the number of families with *CEP164* mutation is small, our findings support a gradient of genotype-phenotype correlations characteristic of NPHP-RC (Table 1), in which null mutations cause the severe dysplastic phenotypes of Meckel syndrome and JS, whereas hypomorphic alleles cause the milder degenerative phenotypes of NPHP and SLSN (Hildebrandt et al., 2011). *CEP164* is transcribed into three common isoforms (Figures S2A–S2C) and is part of the photoreceptor sensory cilium proteome (Liu et al., 2007). To study subcellular localization of the CEP164 protein, we utilized antibodies against human CEP164 for immunoblotting and immunofluorescence (Figure S3).

Mutation of *CEP164* Interferes with Ciliogenesis

By confocal microscopy of GFP-labeled CEP164 protein with other labels, we show that CEP164 colocalizes in hTERT-RPE cells with the mother centriole, with the mitotic spindle poles, and with the abscission structure in a cell-cycle-dependent way (Figure S4), a feature characteristic of proteins involved in single-gene ciliopathies (Otto et al., 2010; Graser

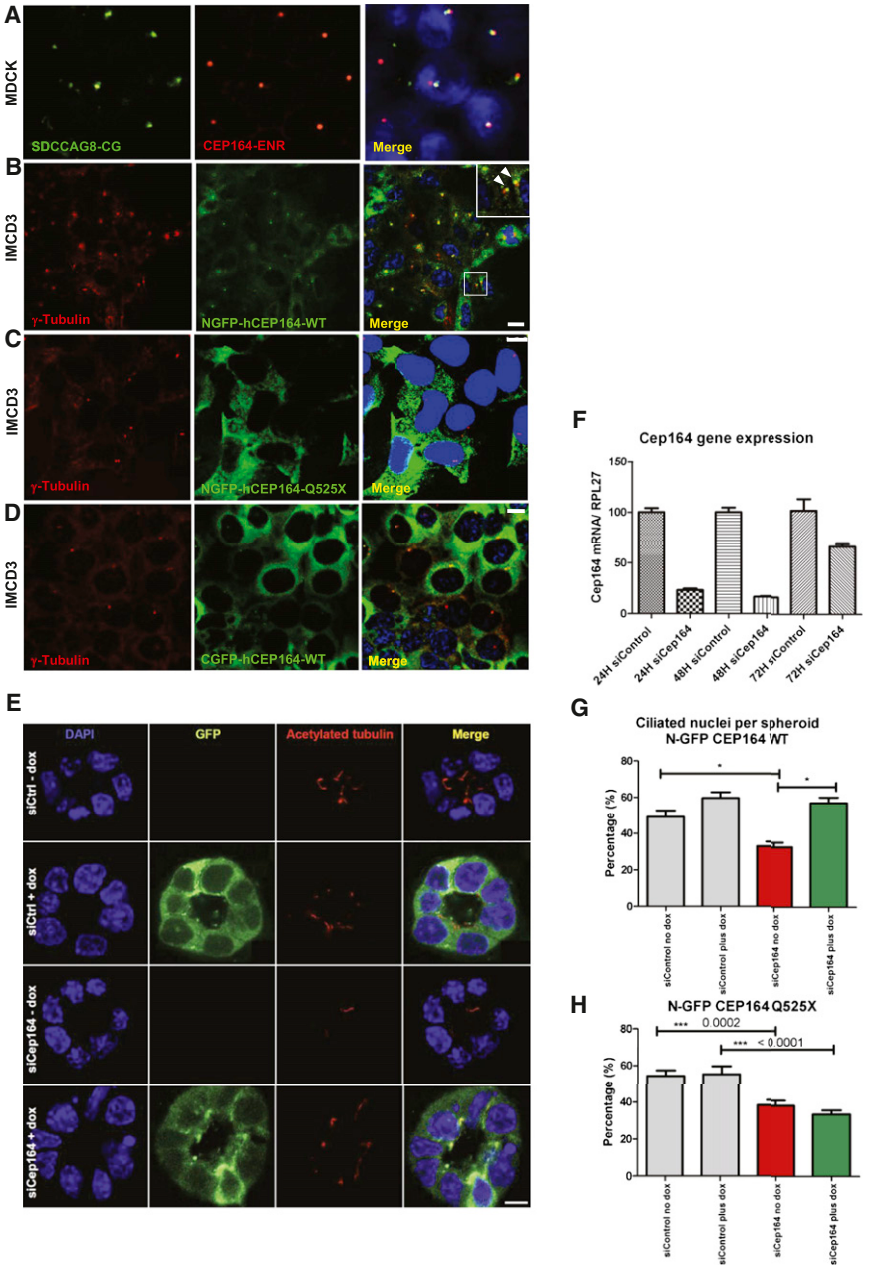

Figure 3. Expression of Mutant *CEP164* in Renal Epithelial Cells Abrogates Localization to Centrosomes

(A) Immunofluorescence using α-SDCCAG8/NPHP10-CG antibody in MDCK cells, labels both centrioles, whereas α-CEP164-ENR antibody demonstrates CEP164 staining at the mother centriole only.

(B) Inducible overexpression of N terminally GFP-tagged human full-length CEP164 isoform 1 (NGFP-CEP164-WT) in IMCD3 cells demonstrates, in addition to a cytoplasmic expression pattern, localization at one of the two centrioles (inset, arrow heads) consistent with selective localization to the mother centriole (Graser et al., 2007). Both centrioles are stained with an anti-γ-tubulin antibody.

(C) In contrast, the centrosomal signal is abrogated upon overexpression of an N terminally GFP-tagged truncated CEP164 construct representing the mutation p.Q525X.

(D) The number of centrosomes positive for CEP164 is reduced upon overexpression of C terminally GFP-tagged human full-length CEP164 isoform 1 (CGFP-hCEP164-WT), which mimics the mutation p.X1460WextX57 that causes a read-through of the stop-codon X1460, adding 57 aberrant amino acid residues to the C terminus of CEP164. Similar data were obtained upon CEP164 expression in hTERT-RPE cells (see also Figures S3B–S3D). IMCD3 cells were stably transfected with the respective *CEP164* constructs in a retroviral vector for doxycyclin-inducible expression (pRetroX-Tight-Pur). Scale bars, 10 μm.

(E–H) Knockdown of *Cep164* disrupts ciliary frequency. (E) Depletion of *Cep164* by siRNA (F) causes a ciliary defect in 3D spheroid growth assays. IMCD3 cells transfected with either siCtrl or *siCep164* were grown to spheroids in 72 hr and immunostained for acetylated tubulin (red). DAPI stains nuclei (blue). Doxycycline induced stably transfected NGFP-hCEP164-WT (green). Space bar represents 5 μm. (G) Nuclei and cilia were scored within a single spheroid to generate ciliary frequencies. si*Cep164* transfected cells manifest lower cilia frequencies (33%) compared to control transfected IMCD3 cells (49%). Induction of NGFP-hCEP164-WT in *siCep164* transfected cells rescues this ciliary defect (57%). 50 spheroids per condition were analyzed in three independent experiments. Error bars represent SEM, n = 3, *p value < 0.0002. (H) Ciliary frequency is not rescued by mutant CEP164. Ciliary frequencies are reduced in si*Cep164* transfected IMCD3 cells (39%) compared to control *siCtrl* transfected IMCD3 cells (54%). Induction of NGFP-hCEP164-Q525X does not rescue this ciliary defect (34%). 50 spheroids per condition were analyzed. Error bars represent SEM, ***p value < 0.0002.

See also Figure S3.

et al., 2007) and that this colocalization is abrogated by mutations (Figure 3, Figures S3C–S3F). We thus demonstrated lack of centrosomal localization for the truncating mutation p.Q525X and for an equivalent of the p.X1460WextX57 mutation.

Loss of function of several genes that cause nephronophthisis in NPHP-RC cause disruption of 3D architecture of renal epithelial cell culture (Otto et al., 2010; Sang et al., 2011). To evaluate CEP164 by this criterion, we transfected murine kidney IMCD3 cells with siRNA oligonucleotides against murine *Cep164*, or random sequences (Ctrl) in 3D spheroid growth assays. Cells transfected with si*Cep164* developed spheroids with overall normal architecture and size, but with markedly reduced frequency of cilia (Figures 3E–3H). We conclude that Cep164 affects ciliogenesis or maintenance but that the overall architecture of renal 3D growths is not as grossly affected as we have previously seen for knockdown of other NPHP-RC genes (Sang et al., 2011).

NPHP-RC Proteins Colocalize with the DDR Protein TIP60 to Nuclear Foci

A noncentrosomal localization for CEP164 was described by demonstrating its translocation to nuclear foci in response to DNA damage (Pan and Lee, 2009; Sivasubramaniam et al., 2008). CEP164 plays a role in DDR signaling where it interacts with the DDR protein ATRIP (Figure S2C), is activated by the DDR proteins ATM and ATR, and is necessary for checkpoint-1 (Chk1) activation. Abrogation of CEP164 function leads to loss of G_2/M cell-cycle checkpoint and aberrant nuclear divisions (Sivasubramaniam et al., 2008).

Localization of SDCCAG8 (alias NPHP10) (Otto et al., 2010), shows nuclear foci in hTERT-RPE cells in addition to its centrosomal localization (Figures 4B–4C). Transient shRNA knockdown confirmed specificity of the signal (Figures S4B–S4D). SDCCAG8/NPHP10 did not colocalize with markers for PLM bodies (Janderová-Rossmeislová et al., 2007) or CENP-C (marking chromosomal centromeres) (Figures S5A and S5B). In contrast, SDCCAG8/NPHP10 fully colocalized with SC35 in hTERT-RPE cells (Figures 4A–4C). SC35, also known as serine/arginine-rich splicing factor 2 (SRSF2), plays a role in DDR by controlling cell fate decisions in response to DNA damaging agents (Edmond et al., 2011; Reinhardt et al., 2011). SC35 marks hubs of enhanced gene expression (Szczerbal and Bridger, 2010), is phosphorylated by topoisomerase I (Elias et al., 2003), and is required for genomic stability during mammalian organogenesis (Xiao et al., 2007). Moreover, ZNF423 also fully colocalizes (Figure 4D), and CEP164 partially colocalizes (Figure 4E) with SC35 in nuclear foci. Consequently, ZNF423 and CEP164 also colocalize with SDCCAG8/NPHP10 in SC35-positive nuclear foci (Figures 4F and 4G).

SC35 functions within a TIP60 complex, in which TIP60 acetylates SC35 on lysine 52 (Figure S1B), modifying the role of SC35 in the promotion of apoptosis and inhibition of G_2/M arrest (Edmond et al., 2011), which is regulated by the checkpoint proteins Chk1 and Chk2 (Figure S1D). Interestingly, the TIP60 protein, together with the heterotrimeric MRN complex (of which MRE11 is a component) constitutes the major activator of ATM within the ATM pathway of DDR signaling (Ciccia and Elledge, 2010) (Figure S1A). In hTERT-RPE cells the ATM activator TIP60 colocalizes to nuclear foci with SC35/SRSF2 (Figure 4H) and partially with the identified NPHP-RC protein CEP164 (Figure 4I). We thus identify a group of NPHP-RC proteins and demonstrate that they colocalize to nuclear foci with the DDR proteins TIP60 and SC35. These gene products include the identified NPHP-RC proteins ZNF423 and CEP164 as well as SDCCAG8/NPHP10. Interestingly, the protein OFD1, which is mutated in the ciliopathy oral-facial-digital syndrome, is part of the TIP60 complex. We recently identified OFD1 as a direct interaction partner of SDCCAG8/NPHP10 (Figure S1B) (Otto et al., 2010).

Cep164 Associates with DDR Proteins and Its Loss Causes DDR Defects

Because one of the central mechanisms controlled by DDR signaling is cell-cycle regulation through phosphorylation of checkpoint-1 (Chk1) and checkpoint-2 (Chk2) proteins (Figure S1D), we tested whether Chk proteins are recruited to SC35/SRSF2-positive nuclear foci. SC35 and p317-Chk1 colocalize to nuclear foci in hTERT-RPE cells (Figure 4J). We then tested whether localization of CEP164 to nuclear foci was inducible by DNA damage. Following irradiation with 20–50 J/m^2 of UV light, CEP164-positive nuclear foci condensed to larger size and colocalized with TIP60 and Chk1 to foci of similar size (Figures 4K–4O). TIP60 and p317-Chk1 colocalized within these foci (Figure 4P). We thus demonstrate that CEP164 translocates in response to DNA damage to nuclear foci that contain the DDR proteins TIP60 and Chk1.

Lagging chromosomes on anaphase spindles (''anaphase lag'') are a hallmark of many mutations that affect mitotic checkpoint integrity. We show that si*Cep164* knockdown in IMCD3 cells increased anaphase lag from 1% in si*Ctrl* controls to 21% in si*Cep164*-treated cells (Figures 5A and 5B, $p = 0.04$). This phenomenon was specific, since doxycycline-inducible expression of *WT-CEP164* during *Cep164* siRNA knockdown reduced the incidence of anaphase lag to just 4% (Figure 5B). These data indicate a requirement for Cep164 at the G_2/M checkpoint.

The DDR pathway can be activated by the CDK inhibitor roscovitine, which also reduces Chk1 expression (Maude and Enders, 2005). Roscovitine reduces the development of kidney cysts in the *Nphp9* mouse model, *Jck* (Bukanov et al., 2006). We therefore tested the influence of roscovitine (targeting CDK2, 5, 7 and 9) on DDR activation in IMCD3 cells. Immunofluorescence shows increased uniform distribution of γH2AX (activated H2AX phosphorylated at Ser139) in the nucleus of IMCD3 cells upon roscovitine treatment in irradiated cells, indicating partial DDR activation (Figure 5C). Second, in cells treated with roscovitine, UV irradiation caused enhanced γH2AX staining with a prominent nuclear foci pattern, characteristic of strong DDR activation (Figure 5D). Immunoblotting showed that roscovitine decreased the amount of CEP164 present in both control and UV-irradiated cells (Figures 5E and 5F). This was most likely due to translocation of CEP164 into the nucleus upon roscovitine treatment, as shown by subcellular fractionation (Figure 5F). As expected, UV radiation increased phosphorylation of Chk1 at Ser317 (p-Chk1) (Figure 5E), and roscovitine decreased Chk1 protein expression and abrogated UV-induced p-Chk1 in both cytoplasm and nucleus (Figures 5G and 5H). These data indicate that CDK inhibition by roscovitine causes nuclear translocation of CEP164 and inhibits Chk1 activation. γH2AX activation by roscovitine may restore cell-cycle control by Chk2 activation instead (Maude and Enders, 2005).

Human Wild-Type *CEP164* but Not Its NPHP-RC Truncation Mutant Rescues IMCD3 Cell Proliferation

In clonally selected IMCD3 cells expressing wild-type human *CEP164* cDNA construct *N-GFP-CEP164-WT* under doxycycline (Dox) control, depletion of endogenous mouse *Cep164* retarded proliferation in comparison to either undepleted control cells or undepleted cells that were Dox-induced to overexpress *N-GFP-CEP164-WT* alone (Figure 5G). Cep164-depleted growth was rescued by Dox-induced expression of human *N-GFP-CEP164-WT* (Figure 5G). Cells expressing truncated cDNA construct *N-GFP-CEP164-Q525X*, modeling the NPHP-RC mutation in family F59, exhibited retarded growth, even when the endogenous Cep164 was present (Figure 5H), consistent with a dominant negative effect. Further depletion of the endogenous

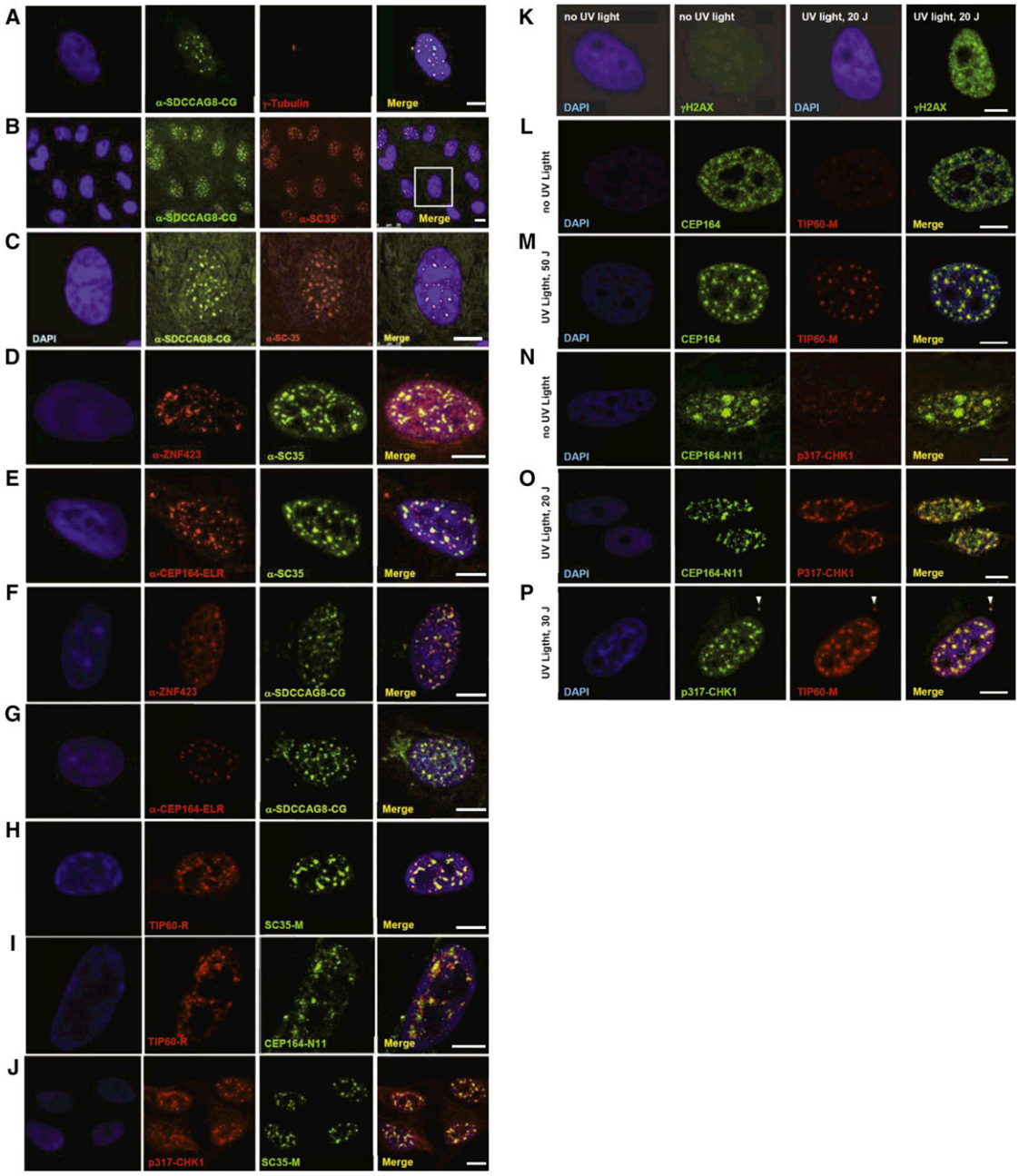

Figure 4. Colocalization upon Immunofluorescence of the NPHP-RC Proteins SDCCAG8/NPHP10, ZNF423 and CEP164 to Nuclear Foci that Are Positive for the DDR Signaling Proteins SC35, TIP60 and Chk1 in hTERT-RPE Cells

(A–G) Colocalization of NPHP-RC proteins with SC35 in nuclear foci. SDCCAG8/NPHP10 (A-C) and ZNF423 (D) fully colocalize to nuclear foci with SC35, and (E) CEP164 partially colocalizes with SC35. SDCCAG8/ NPHP10 also colocalizes with the identified NPHP-RC proteins ZNF423 (F) and CEP164 (G).

(H–J) Colocalization of NPHP-RC proteins with the DDR protein TIP60 and Chk1 to nuclear foci. (H) TIP60 fully colocalizes with SC35. (I) TIP60 partially colocalizes with CEP164. (J) Chk1 fully colocalizes with SC35/ SRSF2. DNA is stained in blue with DAPI. Scale bars, 5 μm.

(K–P) Colocalization of DDR and NPHP proteins upon induction of DDR by UV radiation in HeLa cells. (K) Following irradiation of HeLa cells with UV light at 20 J/m^2 a strong immunofluorescence signal of an anti-γH2AX antibody indicates activation of DDR. (L–M) Upon irradiation with UV light, CEP164-positive nuclear foci condense and colocalize with TIP60 foci of similar size. (N–O) In untreated cells (N) a pattern of broad CEP164 speckles, which are Chk1-negative and locate to DAPI-negative domains, changes to a pattern of multiple smaller foci (O) that are double positive for both CEP164-N11 and Chk1. (P) p317-Chk1 fully colocalizes with TIP60 to nuclear foci and to the centrosome (arrowhead).

See also Figures S4, S5A, and S5B.

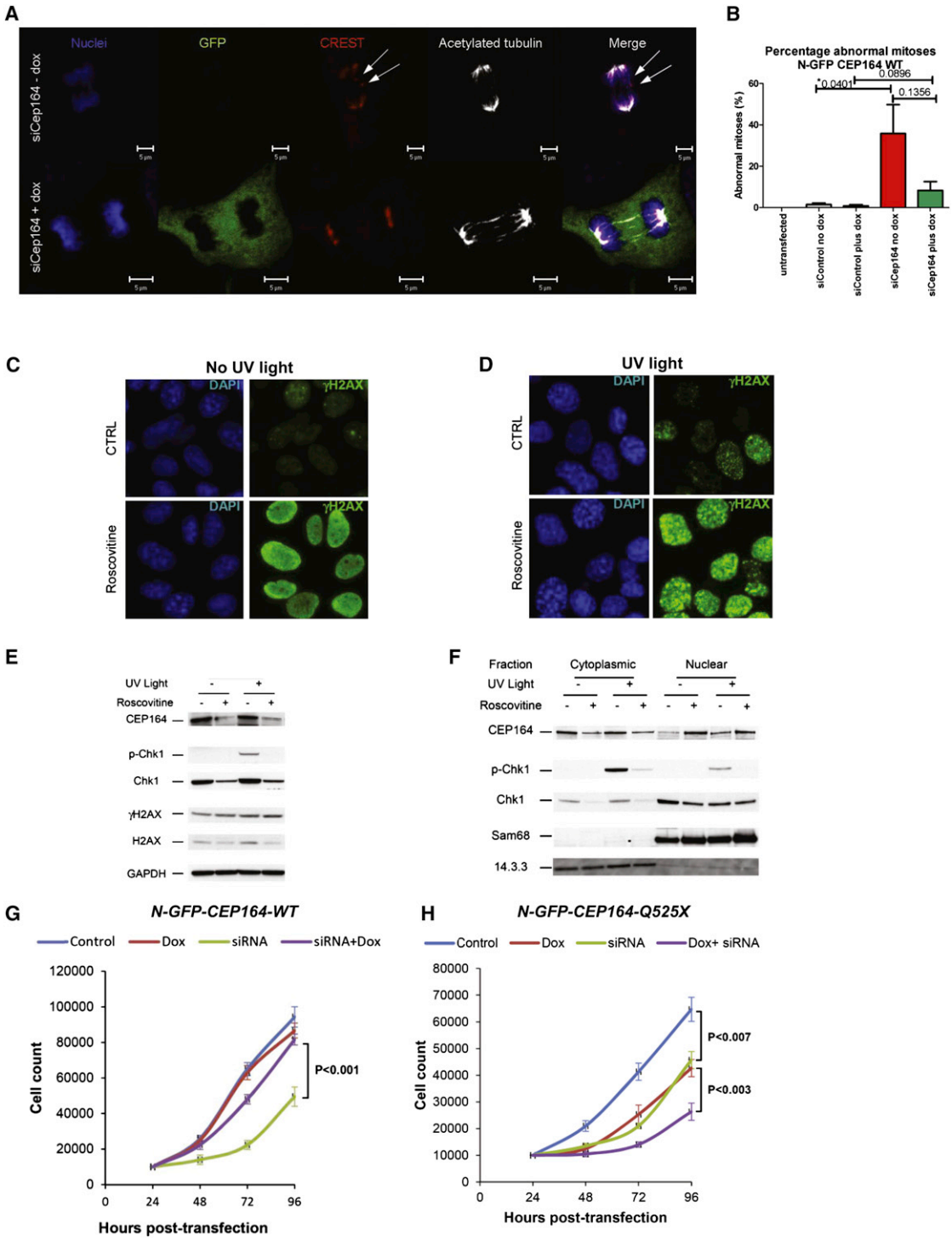

Figure 5. Knockdown of *Cep164* Causes Anaphase Lag and Retarded Cell Growth

(A and B) Knockdown of *CEP164* causes anaphase lag. si*Cep164* knockdown in IMCD3 cells increased anaphase lag incidence from 1% after si*Ctrl* to 21% after si*Cep164*-treated cells (n > 250 anaphases, five independent experiments). CREST antiserum (red) and DAPI (blue) confirmed the presence of incomplete mitotic congression and unattached kinetochores during late anaphase (white arrows). Doxycycline-inducible expression of *WT-CEP164* during *Cep164* siRNA knockdown reduced the incidence of anaphase lag to 4%, whereas untransfected IMCD3 cells had no detectable anaphase lag (0%) (B). Bars represent SEM, p values (Student's t test) are indicated above the bar graph.

(C–F) The effect of roscovitine on UV-induced DDR. Cells were UV irradiated with 30 J/m^2 and analyzed 1 hr after UV irradiation. Where indicated, cells were preincubated for 24 hr with the CDK inhibitor roscovitine (80 μM). (C and D) Immunofluorescence analysis showed that roscovitine triggered uniform nuclear

Cep164 in *N-GFP-CEP164-Q525X*-expressing cells showed an additive effect on growth retardation, confirming the dominant negative effect of *N-GFP-CEP164-Q525X* in this experimental system (Figure 5H).

CEP164 Directly Interacts with CCDC92 and TTBK2

NPHP-RC proteins are known to interact with other NPHP-RC proteins in the dynamic "NPHP-JS-MKS interaction network" (Sang et al., 2011).To identify novel direct interaction partners of CEP164, we performed yeast two-hybrid screening. We identified CCDC92 and TTBK2 as direct interactors of CEP164 (Figures S5C–S5J). Interactions between CEP164 and both partners were validated by GST pull-down (Figure S5D) and coimmunoprecipitation (Figures S5E–S5H). Immunofluorescence showed that CCDC92 fully colocalizes with CEP164 at the mother centriole (Figures S5I and S5J).

CEP164 also interacted with NPHP3 and weakly with NPHP4 (Figures S6A–S6B), demonstrating that CEP164 is in a complex with other known NPHP-RC proteins (Figures S1A and S1B). The DDR protein DDB1 interacted with NPHP2 (Figures S6C and S6D). The disheveled protein (Dvl), which is a central component of the Wnt pathway, interacts with NPHP2/inversin targeting Dvl for proteasomal degradation, thereby triggering a switch from canonical to noncanonical Wnt signaling (Germino, 2005; Simons et al., 2005). We identify interaction between Dvl3 and CEP164 (Figures S6E–S6H). Immunocytochemistry reveals that endogenous Dvl3 and CEP164 share centrosomal localization (Figure S6E). We demonstrate that GST-CEP164 (aa 2–195) is sufficient to pull down endogenous Dvl3 from the cellular lysate (Figure S6F). Domain mapping for Dvl3 suggests that CEP164 interacts with the proline-rich region of Dvl3, because only mutants containing this sequence efficiently coimmunoprecipitate with CEP164-GFP (Figure S6G). Interestingly, only wild-type CEP164-mCherryRFP but not the NPHP-RC causing mutant CEP164-Q525X detected in family F59 (Table 1) can be efficiently immunoprecipitated with Dvl3 (Figure S6H), further supporting its pathogenic role.

cep164 Loss of Function Causes NPHP-RC and DDR Activation in Zebrafish

To test in a vertebrate model whether loss of *cep164* function results in both, an NPHP-RC phenotype as well as DDR activation, we performed *cep164* knockdown in zebrafish embryos using morpholino-oligonucleotides (MOs) (Figure 6). A *p53* MO was injected to reduce off-target MO effects (Robu et al., 2007). At 28 hr postfertilization (hpf) we observed the ciliopathy phenotypes of ventral body axis curvature and cell death (Figure 6A–6C). Embryos showed increased expression of phosphorylated γH2AX (Figures 6D and 6E). At 48 hpf, *cep164* morphants displayed the typical ciliopathy phenotype of abnormal heart looping (Figures 6F–6I). At 72 hpf, embryos developed further NPHP-RC phenotypes, including pronephric tubule cysts (Figures 6J and 6K), hydrocephalus, and retinal dysplasia (Figures 6L–6M).

Depletion of CEP164 or *ZNF423(Zfp423)* Causes Sensitivity to DNA Damaging Agents

To assess whether depletion of *CEP164* causes sensitivity to DNA damage, *Cep164* expression was stably suppressed in the mouse renal cell line IMCD3 (Figures 6P and 6Q). *Cep164* knockdown resulted in a dose-dependent increase of γH2AX intensity levels in a FACS analysis, signifying increased radiation sensitivity to IR and perturbed DDR. Cellular sensitivity to IR was also seen in cells depleted of *CEP164* using a multicolor competition assay (MCA) (Smogorzewska et al., 2007) (Figures S7A and S7B).

To test whether *ZNF423*(*Zfp423*) affects DDR, we examined P19 cells, which express high levels of endogenous *Zfp423* (Figures 6R–6T). Replicate cultures infected with lentivirus expressing either scrambled control or *Zfp423*-targeted shRNA were exposed to 0–10 Gy of X-irradiation and imaged for Zfp423 and nuclear γH2AX foci (Figure 6R). Quantification showed significantly increased γH2AX intensities in *Zfp423*-depleted cells at lower (0.5 and 1.0 Gy) exposures (Figure 6S), but the effect was nonsignificant when corrected for the number of exposures. To determine whether sensitivity to lower dose is reproducible, we exposed 32 additional cultures at 1.0 Gy (Figure 6T). Normalized γH2AX fluorescence in *Zfp423* knockdown had both higher mean (9.6 versus 4.7) and median (6.6 versus 5.2) values than control (Figure 6T). These data replicate the radiation sensitivity with high significance ($p = 0.018$, Mann-Whitney U test, 2 tails), indicating that P19 cells require Zfp423 for quantitatively normal DDR. These results are further confirmed by multicolor competition assays Figure S7C.

DISCUSSION

Disease Gene Identification Implicates NPHP-RC Proteins in DDR

Many DDR signaling proteins localize to nuclear foci and to centrosomes. In addition, dual localization of proteins at

distribution of γH2AX (activated H2AX phosphorylated at Ser139) in non-UV irradiated cells suggesting partial DDR activation (C). UV radiation caused enhanced γH2AX staining with a prominent nuclear foci pattern, characteristic of strong DDR activation (D). (C and D) Error bars denote SEM.

(E and F) The effect of roscovitine on UV-triggered subcellular localization of CEP164 and Chk1. CEP164 and Chk1 proteins, along with nuclear marker Sam68 and cytoplasmic marker 14.3.3 were analyzed by Western blot. Roscovitine decreased the amount of CEP164 present in control and UV-irradiated cells (E). This was most likely due to translocation of CEP164 into the nucleus upon roscovitine treatment as shown by subcellular fractionation (F). As expected, UV radiation increased phosphorylation of Chk1 at Ser317 (p-Chk1) (E), and roscovitine decreased Chk1 protein expression and abrogated UV-induced p-Chk1 in both cytoplasm and nucleus (E-F). Proteins 14.3.3 and Sam68 serve as controls for cytoplasmic versus nuclear fraction, respectively. See also Figure S6.

(G and H) Transient knockdown of *Cep164* inhibits proliferation, which is rescued by wild-type but not mutant CEP164. In clonally selected and doxycycline (Dox)-inducible mouse IMCD3 cells siRNA knockdown was performed. (G) IMCD3 cells depleted of murine *Cep164* grew more slowly (siRNA, green line) than nondepleted cells (control, blue line) or the nondepleted cells induced to express human wild-type CEP164 (Dox, red line). Expression of WT *Cep164* in siRNA-depleted cells rescued the slow growth phenotype of *Cep164* depletion (siRNA$^+$dox, purple line). (H) As in (G), except mutant *Cep164* cDNA (*CEP164-Q525X*) was expressed under doxycyclin control. Expression of this allele itself had a negative impact on cell growth (green line), suggesting a dominant negative effect. An even greater negative effect was seen when the endogenous Cep164 was depleted in cells expressing *CEP164-Q525X* (siRNA$^+$dox, purple line). The average counts are plotted with standard deviations. Asterisks indicate significant differences by unpaired Student's t test ($p < 0.05$).

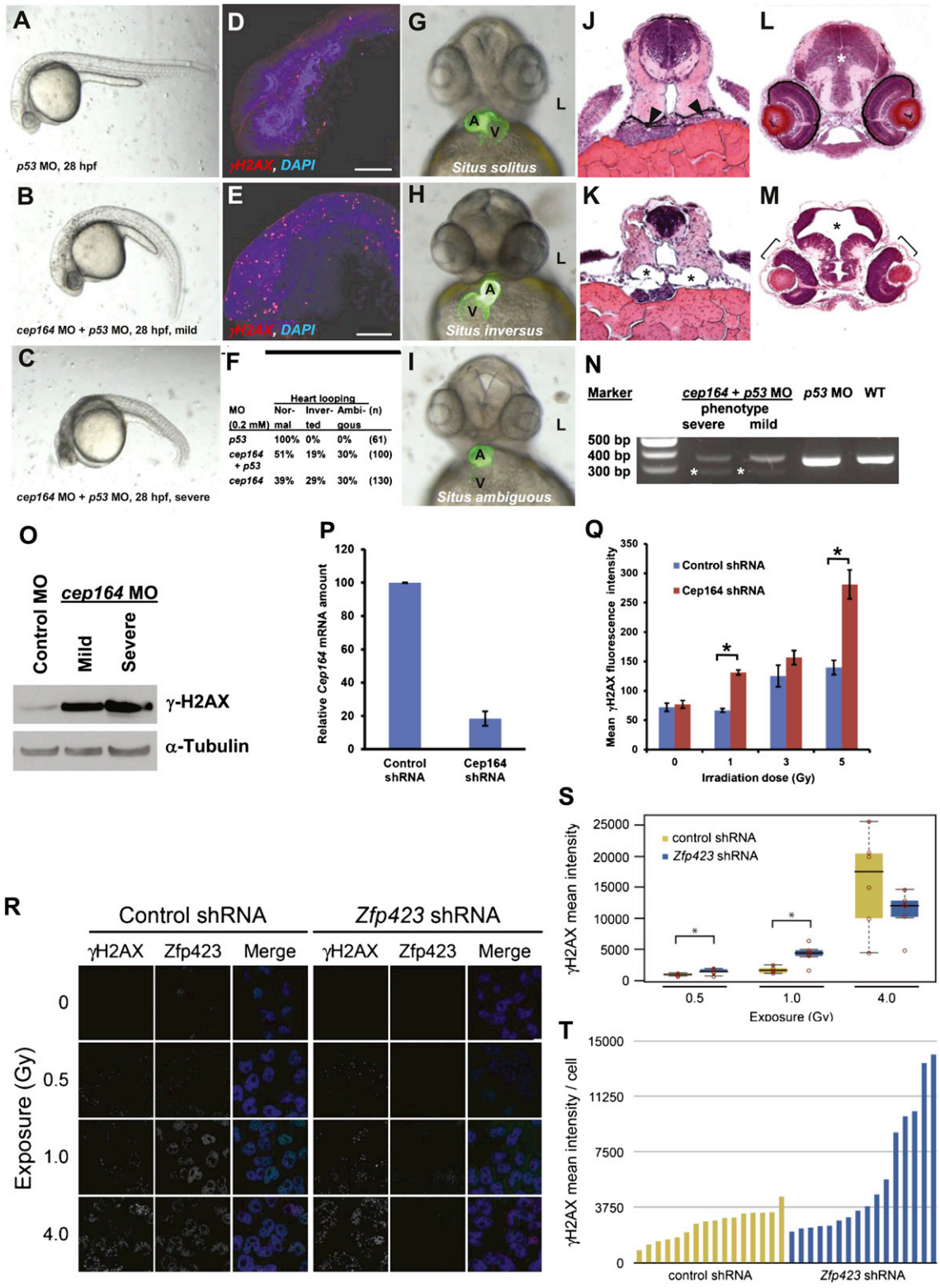

Figure 6. Knockdown of *cep164* in Zebrafish Embryos Results in Ciliopathy Phenotypes, and Knockdown of *Cep164* or *Zfp423(Znf423)* Causes Sensitivity to DNA Damage

A morpholino-oligonucleotide (*cep164* MO) targeting the exon 7 splice donor site of zebrafish *cep164* was injected into fertilized eggs at the one to four-cells stage together with *p53* MO (0.2 mM) to minimize nonspecific MO effects.

centrosomes and at nuclear foci has been demonstrated for multiple known DDR proteins related to ataxia or CVH. Individuals with mutations in the three NPHP-RC-causing genes that we identify here, *MRE11*, *ZNF423*, and *CEP164*, share the NPHP-RC phenotypes of CVH and ataxia. The first protein that strongly linked DDR signaling to the ataxia phenotype was the protein ATM (ataxia telangiectasia mutated) (Savitsky et al., 1995). Interestingly, we identify here in individuals with NPHP-RC, CVH and ataxia, mutations in proteins that colocalize to nuclear foci with TIP60 and/or its interaction partner SC35. These proteins are ZNF423, CEP164, and the previously identified NPHP-RC protein SDCCAG8/NPHP10 (Otto et al., 2010).

Our findings support the notion that many products of genes, which if mutated cause NPHP-RC and/or ataxia, play a role in DDR and are part of a dynamic protein complex.

A DDR-Based Pathogenic Hypothesis of Dysplasia and Degeneration in NPHP-RC

We here generate evidence that NPHP-RC proteins exhibit dual localization at centrosomes and in nuclear foci and that they play a role in DDR. We also demonstrate the parallel occurrence of DDR defects with an NPHP-RC phenotype upon *cep164* knockdown in zebrafish. We therefore propose that defects in DDR may participate in the pathogenesis of NPHP-RC. Whereas multiple signaling pathways have been implicated in the pathogenesis of NPHP-RC (Hildebrandt et al., 2011), including noncanonical (Simons et al., 2005) and canonical Wnt signaling (Yu et al., 2009), Shh signaling (Huangfu et al., 2003), and mitotic spindle orientation (Fischer et al., 2006), none of them consistently explains the phenotypes observed. In particular, none of these mechanisms provides a model for the dichotomy of dysplasia phenotypes resulting from null-alleles of *NPHP-RC* genes versus degenerative phenotypes resulting from hypomorphic alleles of the same *NPHP-RC* genes. Based on our findings we here propose a pathogenic hypothesis for NPHP-RC that implicates DDR signaling as a relevant disease mechanism. Within this hypothesis, loss of function of NPHP-RC proteins with a dual role in DDR and centrosomal signaling, would cause disturbance of cell-cycle checkpoint control, which is particularly detrimental for embryonic and adult progenitor cell survival. This notion is in accordance with the orthologous mouse model for *ZNF423* loss of function, the *Zfp423*$^{-/-}$ mouse, in which CVH with ataxia is caused by defective granule progenitor proliferation in the cerebellum (Alcaraz et al., 2006).

Within this pathogenic hypothesis for NPHP-RC, a DDR signaling defect would lead to impairment of cell-cycle checkpoint control, which in turn would cause lack of progenitor cells. This hypothesis could lend a possible explanation to the following persisting conundrum of NPHP-RC pathogenesis: in certain NPHP genes (e.g., NPHP3, 6, or 8) *null mutations* cause severe, congenital-onset phenotypes of dysplasia and malformation in kidney, eye, CVH, and liver, whereas *hypomorphic mutations* in the same gene cause only late-onset degenerative phenotypes such as renal tubular degeneration and fibrosis (nephronophthisis), retinal degeneration (Senior-Loken syndrome), and liver fibrosis. However, the disease mechanisms of neither the degenerative nor the dysplastic phenotypes are understood. These findings suggest that null mutations act during morphogenesis in embryonic development causing dysplasia and malformation, whereas hypomorphic mutations act during the "chronic" processes of tissue maintenance and repair, which are spread out over months or years of the life of an organism. Because DDR signaling is in high demand under conditions of high proliferation during development (morphogenesis), causing high "replication stress" to progenitor cells, tissue dysplasia would be an expected pathogenic outcome. Conversely, during tissue maintenance, low replication stress would be expected, but persistent DDR impairment would allow

(A–E) Whereas *p53* MO injection (n = 67) did not produce any phenotype (A), coinjection of *cep164* MO at 28 hpf caused the mild ciliopathy phenotype of ventral body axis curvature in 48% of embryos (60/125) (B). 50% of embryos (62/125) showed severe cell death throughout the body as judged by gray-appearing cells in the head region (C). Embryos with severe cell death also showed increased expression of phosphorylated γH2AX (D) compared to *p53* MO control (E). Most embryos with massive cell death did not survive beyond 48 hpf.

(F–I) At 48 hpf, surviving *cep164* morphants displayed the ciliopathy phenotype of laterality defects. Whereas *p53* MO did not cause any abnormal heart looping (F and G), *cep164* MO caused inverted heart looping (H) or ambiguous heart looping (I). (A, atrium; L, left; V, ventricle).

(J–M) At 72 hpf, *cep164* morphant embryos developed further ciliopathy phenotypes. When compared to *p53* MO controls (J), pronephric tubules (arrow heads) exhibited cystic dilation (K), asterisks) in 25% (7/28) of embryos, compared to *p53* MO controls (J and L), 0% (0/67) of which showed kidney cysts, hydrocephalus (asterisk), or retinal dysplasia (brackets) (M).

(N) At 0.2 mM, *cep164* MO knockdown effectively altered mRNA processing as revealed by RT-PCR. The wild-type (WT) mRNA product is 339 bp. A shorter aberrantly spliced mRNA product appeared in *cep164* morphants (asterisks), and the normal mRNA product was significantly reduced. *p53* MO alone did not affect *cep164* mRNA processing.

(O) Quantification of γ-H2AX levels in *cep164* MO morphants. Whole-fish lysates were prepared from morphants injected with control MO (p53 0.2 mM) or *cep164* MO (p53 0.2 mM, *cep164* 0.2 mM). Injection of *cep164*-targeting MO causes upregulation of γ-H2AX in *cep164* morphant embryos signifying perturbed DDR. γ-H2AX levels correlate with the phenotypic severity of the *cep164* morphants (see A–C). Anti-α-tubulin antibody was used to show equal loading.

(P and Q) *Cep164*-deficient IMCD3 cells exhibit radiation sensitivity. In IMCD3 cells transduced with shRNA retrovirus, *Cep164* expression was suppressed by shRNA knockdown to about 20% of control as judged by qPCR (P). *Cep164* knockdown resulted in a dose-dependent increase of γH2AX-positive cells in a FACS assay, signifying increased radiation sensitivity to IR and perturbed DDR. See also Figure S7. In (Q) the level of significance of two-tailed t test ($p < 0.001$) is indicated by an asterisk. Error bars denote SEM.

(R–T) *Zfp423(Znf423)*-deficient P19 cells exhibit radiation sensitivity. P19 cells transduced with shRNA lentivirus were exposed to the indicated level X-irradiation. Zfp423 and γH2AX immunofluorescence was quantified in matched replicate cultures for each virus 2 hr after irradiation. (R) Representative images illustrate dose-responsiveness of γH2AX and effective knockdown of *Zfp423* expression. (S) γH2AX intensity normalized to DAPI$^+$ nuclei is increased following IR at 0.5 and 1.0 Gy, signifying increased IR sensitivity and perturbed DDR (2 fields from each of 6 replicate cultures per condition). Asterisks, uncorrected pair-wise $p < 0.05$, Mann-Whitney U test, 2 tails. (T) Histogram shows average γH2AX intensity per cell in 16 additional replicate cultures for each shRNA at 1.0 Gy exposure. $p = 0.018$, Mann-Whitney U test, 2 tails. See also Figure S7. Box plots delimit quartiles in (S).

slow accumulation of DNA damage with a phenotype of tissue degeneration.

At least two related findings support this model: (1) In a mouse conditional knockout model of the cystic kidney disease gene *Pkhd1*, knockout of the gene before 2 weeks of postnatal life, up to which a high proliferation state prevailed, caused (dysplastic) kidney cysts, whereas knockdown after 2 weeks of postnatal life, when proliferation rate was shown to be dramatically reduced, only caused occasional cysts, the number of which increased when tissue injury was induced (Piontek et al., 2007). This phenomenon could be explained by different degrees of replication stress, and thereby DDR activation, under different proliferation rates. (2) In Seckel syndrome (primordial dwarfism), a progeria syndrome with CVH caused by mutation of the centrosomal and DDR proteins ATR, CEP152, or pericentrin, the degree of cerebellar impairment is dependent on cell proliferation state (Kalay et al., 2011; Murga et al., 2009; Rauch et al., 2008).

A DDR-Based Pathogenic Hypothesis Might Explain Specific Organ Involvement in NPHP-RC

Regarding the question why organ degeneration occurs in specific organs and at characteristic sites, it is tempting to speculate that the specific tissue regions or cell types affected in NPHP-RC are more strongly exposed to genotoxins. In the kidney, the distal convoluted tubule segment, around which most fibrotic changes occur, is more strongly exposed to genotoxins such as hydroxyurea. Retinal degeneration could be caused by postnatal accumulation of UV light-induced DNA damage. Most strikingly, bile duct-surrounding cholangiocytes in the liver are the one mammalian cell type that is most strongly exposed to genotoxins that are generated by the liver for excretion in bile.

In summary, a testable pathogenic hypothesis of NPHP-RC that implicates DDR signaling, impaired cell-cycle checkpoint control with lack of progenitor cells might potentially explain some of the ill understood features of ciliopathies:

(1) It might provide a mechanism for the dual phenotypes of degeneration/dysplasia seen in NPHP-RC in kidney, eye, cerebellum and liver.
(2) It would implicate in the NPHP-RC pathogenesis, lack of response to replication stress-sensing as a functional basis for understanding the dualism of dysplasia that occurs in high-proliferation states during development/morphogenesis or repair versus degeneration, which occurs during the low proliferation state of tissue maintenance.
(3) It would characterize the degenerative phenotypes as diseases of "organ-specific premature aging," thereby pointing in new directions for identification of small compounds for therapy including cyclin inhibitors.

EXPERIMENTAL PROCEDURES

Research Subjects

We obtained human samples following informed consent from individuals with NPHP-RC. Approval for human subjects research was obtained from the University of Michigan Institutional Review Board and the other institutions involved. The diagnosis of NPHP-RC was based on published clinical criteria (Chaki et al., 2011).

Linkage Analysis

For genome-wide HM the GeneChip Human Mapping 250k *Sty*I Array from Affymetrix was used. Nonparametric LOD scores were calculated using a modified version of the programs GENEHUNTER 2.1 (Kruglyak et al., 1996; Strauch et al., 2000) and ALLEGRO (Gudbjartsson et al., 2000) in order to identify regions of homozygosity as described (Hildebrandt et al., 2009; Sayer et al., 2006).

Bioinformatics

Genetic location is according to the February 2009 Human Genome Browser data (http://www.genome.ucsc.eduH).

Immunoblotting and Immunoprecipitation

Immunoblotting and immunoprecipitation were performed as previously described (Bryja et al., 2007). HEK293 cells were transfected with the indicated constructs and lysed 48 hr later. Samples were analyzed using SDS-PAGE and western blotting, or subjected to immunoprecipitation. The antibodies used for immunoprecipitation are described in Extended Experimental Procedures.

cep164 Zebrafish Morpholino Oligo-Mediated Knockdown

MOs were obtained from Gene Tools, LLC (Philomath, OR). MOs (*cep164* at 0.1 mM, standard control at 0.2 mM, and *p53* MO at 0.2 mM) were injected into zebrafish embryos at 1–4 cell stages. Embryos were fixed at 27 hpf with 4% PFA/PBS +1% DMSO overnight, permeablized with acetone at −20°C for 7 min, and stained with antibody against phosphorylated zebrafish γH2AX (1:1,000, gift from Amatruda lab at UT Southwestern) or antibody against cleaved Caspase-3 (1:200, BD Biosciences). Alex568-anti rabbit IgG was used at 1:2,000 and 1:1,000 respectively. The IF procedure followed standard protocol. Morpholinos were: cep164 MO: 50-TATATGCTCTTCTCCATC ACCTCAT; p53 MO: 50-GCGCCATTGCTTTGCAAGAATTG. For histological analyses, embryos were fixed at 72 hpf with 4% PFA/PBS and embedded in JB-4 resin (PolySciences) following the manufacturer's protocol. Six millimeter sections were obtained using a Leica R2265 microtome and stained with hematoxylin-eosin following published procedures (Zhou et al., 2010).

Statistical Analysis

Student's two-tailed nonpaired t tests and normal distribution two-tailed z tests were carried out using pooled standard error and S.D. values to determine the statistical significance of different cohorts.

SUPPLEMENTAL INFORMATION

Supplemental Information includes Extended Experimental Procedures, seven figures, and two tables and can be found with this article online at http://dx.doi.org/10.1016/j.cell.2012.06.028.

ACKNOWLEDGMENTS

We are grateful to the study individuals for their contributions. This research was supported by grants from the NIH to F.H. (DK068306, DK090917), B.A.H (NS054871, NS060109), N.K. (HD042601, DK075972, DK072301), and W.Z. (DK091405); the March of Dimes Foundation and the Center for Organogenesis of the University of Michigan to F.H.; the Netherlands Organization for Scientific Research to R.R. (NWO Vidi-91786396) and R.H.G. (NWO Vidi-917.66.354), the Avenir-INSERM program, the Agence Nationale pour la Recherche, the Union Nationale pour les Aveugles et Déficients Visuels, RETINA France, Programme Hospitalier de Recherche National 2007, and the Association Bardet-Biedl, France to H.D. and C.S.; the European Community's Seventh Framework Programme FP7/2009 under grant agreement no: 241955, SYSCILIA (to R.H.G., G.G.S., N.K., R.R., H.O., C.A.J. and G.W.); the Dutch Kidney Foundation (KJPB09.009 and IP11.58 to H.H.A); the Retina Research Foundation and the National Eye Institute (R01EY018571) to R.C.;

the NIH to H.W. (F32EY19430); and the DFG (SCHE1562 and SFB832 to B.S.; SFB829 to T.B.; SFB592 to H.O.). R.K.K. is supported by FFB-Canada, CIHR, FRSQ, and Reseau Vision. J.S.A. is supported by the Lundbeck Foundation. V.B. is supported by MSM0021622430 (Ministry of Education, Youth and Sports of the Czech Republic), 204/09/H058, and 204/09/0498 (Czech Science Foundation) and EMBO Installation Grant; I.C. is supported by the programme, Brno PhD Talent of South Moravian Center for International Mobility. S.S. is a laureate of the "Equipe FRM" (DEQ20071210558) and the Agence National de la Recherche (R09087KS, R11012KK). W.Z. is a Carl. W. Gottschalk research scholar of the American Society of Nephrology. J.A.S. is a GlaxoSmithKline clinician scientist. A.S. is supported by the Burroughs Wellcome Fund Career Award for Medical Scientists and the Doris Duke Charitable Foundation Clinical Scientist Development Awards and is a Rita Allen Foundation and an Irma T. Hirschl scholar. F.H. is an Investigator of the Howard Hughes Medical Institute, a Frederick G. L. Huetwell Professor, and a Doris Duke Distinguished Clinical Scientist.

Received: September 4, 2011
Revised: February 1, 2012
Accepted: June 25, 2012
Published: August 2, 2012

REFERENCES

Alcaraz, W.A., Gold, D.A., Raponi, E., Gent, P.M., Concepcion, D., and Hamilton, B.A. (2006). Zfp423 controls proliferation and differentiation of neural precursors in cerebellar vermis formation. Proc. Natl. Acad. Sci. USA *103*, 19424–19429.

Alcaraz, W.A., Chen, E., Valdes, P., Kim, E., Lo, Y.H., Vo, J., and Hamilton, B.A. (2011). Modifier genes and non-genetic factors reshape anatomical deficits in Zfp423-deficient mice. Hum. Mol. Genet. *20*, 3822–3830.

Ansley, S.J., Badano, J.L., Blacque, O.E., Hill, J., Hoskins, B.E., Leitch, C.C., Kim, J.C., Ross, A.J., Eichers, E.R., Teslovich, T.M., et al. (2003). Basal body dysfunction is a likely cause of pleiotropic Bardet-Biedl syndrome. Nature *425*, 628–633.

Attanasio, M., Uhlenhaut, N.H., Sousa, V.H., O'Toole, J.F., Otto, E., Anlag, K., Klugmann, C., Treier, A.C., Helou, J., Sayer, J.A., et al. (2007). Loss of GLIS2 causes nephronophthisis in humans and mice by increased apoptosis and fibrosis. Nat. Genet. *39*, 1018–1024.

Blachon, S., Gopalakrishnan, J., Omori, Y., Polyanovsky, A., Church, A., Nicastro, D., Malicki, J., and Avidor-Reiss, T. (2008). Drosophila asterless and vertebrate Cep152 Are orthologs essential for centriole duplication. Genetics *180*, 2081–2094.

Bryja, V., Schulte, G., Rawal, N., Grahn, A., and Arenas, E. (2007). Wnt-5a induces Dishevelled phosphorylation and dopaminergic differentiation via a CK1-dependent mechanism. J. Cell Sci. *120*, 586–595.

Bukanov, N.O., Smith, L.A., Klinger, K.W., Ledbetter, S.R., and Ibraghimov-Beskrovnaya, O. (2006). Long-lasting arrest of murine polycystic kidney disease with CDK inhibitor roscovitine. Nature *444*, 949–952.

Chaki, M., Hoefele, J., Allen, S.J., Ramaswami, G., Janssen, S., Bergmann, C., Heckenlively, J.R., Otto, E.A., and Hildebrandt, F. (2011). Genotype-phenotype correlation in 440 patients with NPHP-related ciliopathies. Kidney Int. *80*, 1239–1245.

Cheng, L.E., Zhang, J., and Reed, R.R. (2007). The transcription factor Zfp423/OAZ is required for cerebellar development and CNS midline patterning. Dev. Biol. *307*, 43–52.

Ciccia, A., and Elledge, S.J. (2010). The DNA damage response: making it safe to play with knives. Mol. Cell *40*, 179–204.

Doxsey, S.J., Stein, P., Evans, L., Calarco, P.D., and Kirschner, M. (1994). Pericentrin, a highly conserved centrosome protein involved in microtubule organization. Cell *76*, 639–650.

Edmond, V., Moysan, E., Khochbin, S., Matthias, P., Brambilla, C., Brambilla, E., Gazzeri, S., and Eymin, B. (2011). Acetylation and phosphorylation of SRSF2 control cell fate decision in response to cisplatin. EMBO J. *30*, 510–523.

Elias, E., Lalun, N., Lorenzato, M., Blache, L., Chelidze, P., O'Donohue, M.F., Ploton, D., and Bobichon, H. (2003). Cell-cycle-dependent three-dimensional redistribution of nuclear proteins, P 120, pKi-67, and SC 35 splicing factor, in the presence of the topoisomerase I inhibitor camptothecin. Exp. Cell Res. *291*, 176–188.

Fischer, E., Legue, E., Doyen, A., Nato, F., Nicolas, J.F., Torres, V., Yaniv, M., and Pontoglio, M. (2006). Defective planar cell polarity in polycystic kidney disease. Nat. Genet. *38*, 21–23.

Germino, G.G. (2005). Linking cilia to Wnts. Nat. Genet. *37*, 455–457.

Graser, S., Stierhof, Y.D., Lavoie, S.B., Gassner, O.S., Lamla, S., Le Clech, M., and Nigg, E.A. (2007). Cep164, a novel centriole appendage protein required for primary cilium formation. J. Cell Biol. *179*, 321–330.

Griffith, E., Walker, S., Martin, C.A., Vagnarelli, P., Stiff, T., Vernay, B., Al Sanna, N., Saggar, A., Hamel, B., Earnshaw, W.C., et al. (2008). Mutations in pericentrin cause Seckel syndrome with defective ATR-dependent DNA damage signaling. Nat. Genet. *40*, 232–236.

Gudbjartsson, D.F., Jonasson, K., Frigge, M.L., and Kong, A. (2000). Allegro, a new computer program for multipoint linkage analysis. Nat. Genet. *25*, 12–13.

Hildebrandt, F., Heeringa, S.F., Rüschendorf, F., Attanasio, M., Nürnberg, G., Becker, C., Seelow, D., Huebner, N., Chernin, G., Vlangos, C.N., et al. (2009). A systematic approach to mapping recessive disease genes in individuals from outbred populations. PLoS Genet. *5*, e1000353.

Hildebrandt, F., Benzing, T., and Katsanis, N. (2011). Ciliopathies. N. Engl. J. Med. *364*, 1533–1543.

Huangfu, D., and Anderson, K.V. (2005). Cilia and Hedgehog responsiveness in the mouse. Proc. Natl. Acad. Sci. USA *102*, 11325–11330.

Huangfu, D., Liu, A., Rakeman, A.S., Murcia, N.S., Niswander, L., and Anderson, K.V. (2003). Hedgehog signalling in the mouse requires intraflagellar transport proteins. Nature *426*, 83–87.

Janderová-Rossmeislová, L., Nováková, Z., Vlasáková, J., Philimonenko, V., Hozák, P., and Hodný, Z. (2007). PML protein association with specific nucleolar structures differs in normal, tumor and senescent human cells. J. Struct. Biol. *159*, 56–70.

Kalay, E., Yigit, G., Aslan, Y., Brown, K.E., Pohl, E., Bicknell, L.S., Kayserili, H., Li, Y., Tüysüz, B., Nürnberg, G., et al. (2011). CEP152 is a genome maintenance protein disrupted in Seckel syndrome. Nat. Genet. *43*, 23–26.

Kruglyak, L., Daly, M.J., Reeve-Daly, M.P., and Lander, E.S. (1996). Parametric and nonparametric linkage analysis: a unified multipoint approach. Am. J. Hum. Genet. *58*, 1347–1363.

Ku, M.C., Stewart, S., and Hata, A. (2003). Poly(ADP-ribose) polymerase 1 interacts with OAZ and regulates BMP-target genes. Biochem. Biophys. Res. Commun. *311*, 702–707.

Liu, Q., Tan, G., Levenkova, N., Li, T., Pugh, E.N., Jr., Rux, J.J., Speicher, D.W., and Pierce, E.A. (2007). The proteome of the mouse photoreceptor sensory cilium complex. Mol. Cell. Proteomics *6*, 1299–1317.

Maude, S.L., and Enders, G.H. (2005). Cdk inhibition in human cells compromises chk1 function and activates a DNA damage response. Cancer Res. *65*, 780–786.

Murga, M., Bunting, S., Montaña, M.F., Soria, R., Mulero, F., Cañamero, M., Lee, Y., McKinnon, P.J., Nussenzweig, A., and Fernandez-Capetillo, O. (2009). A mouse model of ATR-Seckel shows embryonic replicative stress and accelerated aging. Nat. Genet. *41*, 891–898.

Ng, S.B., Turner, E.H., Robertson, P.D., Flygare, S.D., Bigham, A.W., Lee, C., Shaffer, T., Wong, M., Bhattacharjee, A., Eichler, E.E., et al. (2009). Targeted capture and massively parallel sequencing of 12 human exomes. Nature *461*, 272–276.

O'Driscoll, M., Ruiz-Perez, V.L., Woods, C.G., Jeggo, P.A., and Goodship, J.A. (2003). A splicing mutation affecting expression of ataxia-telangiectasia and Rad3-related protein (ATR) results in Seckel syndrome. Nat. Genet. *33*, 497–501.

Otto, E.A., Hurd, T.W., Airik, R., Chaki, M., Zhou, W., Stoetzel, C., Patil, S.B., Levy, S., Ghosh, A.K., Murga-Zamalloa, C.A., et al. (2010). Candidate exome capture identifies mutation of SDCCAG8 as the cause of a retinal-renal ciliopathy. Nat. Genet. *42*, 840–850.

Otto, E.A., Ramaswami, G., Janssen, S., Chaki, M., Allen, S.J., Zhou, W., Airik, R., Hurd, T.W., Ghosh, A.K., Wolf, M.T., et al; GPN Study Group. (2011). Mutation analysis of 18 nephronophthisis associated ciliopathy disease genes using a DNA pooling and next generation sequencing strategy. J. Med. Genet. *48*, 105–116.

Pan, Y.R., and Lee, E.Y. (2009). UV-dependent interaction between Cep164 and XPA mediates localization of Cep164 at sites of DNA damage and UV sensitivity. Cell Cycle *8*, 655–664.

Piontek, K., Menezes, L.F., Garcia-Gonzalez, M.A., Huso, D.L., and Germino, G.G. (2007). A critical developmental switch defines the kinetics of kidney cyst formation after loss of Pkd1. Nat. Med. *13*, 1490–1495.

Rauch, A., Thiel, C.T., Schindler, D., Wick, U., Crow, Y.J., Ekici, A.B., van Essen, A.J., Goecke, T.O., Al-Gazali, L., Chrzanowska, K.H., et al. (2008). Mutations in the pericentrin (PCNT) gene cause primordial dwarfism. Science *319*, 816–819.

Reinhardt, H.C., Cannell, I.G., Morandell, S., and Yaffe, M.B. (2011). Is post-transcriptional stabilization, splicing and translation of selective mRNAs a key to the DNA damage response? Cell Cycle *10*, 23–27.

Robu, M.E., Larson, J.D., Nasevicius, A., Beiraghi, S., Brenner, C., Farber, S.A., and Ekker, S.C. (2007). p53 activation by knockdown technologies. PLoS Genet. *3*, e78.

Sang, L., Miller, J.J., Corbit, K.C., Giles, R.H., Brauer, M.J., Otto, E.A., Baye, L.M., Wen, X., Scales, S.J., Kwong, M., et al. (2011). Mapping the NPHP-JBTS-MKS protein network reveals ciliopathy disease genes and pathways. Cell *145*, 513–528.

Savitsky, K., Bar-Shira, A., Gilad, S., Rotman, G., Ziv, Y., Vanagaite, L., Tagle, D.A., Smith, S., Uziel, T., Sfez, S., et al. (1995). A single ataxia telangiectasia gene with a product similar to PI-3 kinase. Science *268*, 1749–1753.

Sayer, J.A., Otto, E.A., O'Toole, J.F., Nurnberg, G., Kennedy, M.A., Becker, C., Hennies, H.C., Helou, J., Attanasio, M., Fausett, B.V., et al. (2006). The centrosomal protein nephrocystin-6 is mutated in Joubert syndrome and activates transcription factor ATF4. Nat. Genet. *38*, 674–681.

Schäfer, T., Pütz, M., Lienkamp, S., Ganner, A., Bergbreiter, A., Ramachandran, H., Gieloff, V., Gerner, M., Mattonet, C., Czarnecki, P.G., et al. (2008). Genetic and physical interaction between the NPHP5 and NPHP6 gene products. Hum. Mol. Genet. *17*, 3655–3662.

Simons, M., Gloy, J., Ganner, A., Bullerkotte, A., Bashkurov, M., Krönig, C., Schermer, B., Benzing, T., Cabello, O.A., Jenny, A., et al. (2005). Inversin, the gene product mutated in nephronophthisis type II, functions as a molecular switch between Wnt signaling pathways. Nat. Genet. *37*, 537–543.

Sivasubramaniam, S., Sun, X., Pan, Y.R., Wang, S., and Lee, E.Y. (2008). Cep164 is a mediator protein required for the maintenance of genomic stability through modulation of MDC1, RPA, and CHK1. Genes Dev. *22*, 587–600.

Smogorzewska, A., Matsuoka, S., Vinciguerra, P., McDonald, E.R., 3rd, Hurov, K.E., Luo, J., Ballif, B.A., Gygi, S.P., Hofmann, K., D'Andrea, A.D., and Elledge, S.J. (2007). Identification of the FANCI protein, a monoubiquitinated FANCD2 paralog required for DNA repair. Cell *129*, 289–301.

Stewart, G.S., Maser, R.S., Stankovic, T., Bressan, D.A., Kaplan, M.I., Jaspers, N.G., Raams, A., Byrd, P.J., Petrini, J.H., and Taylor, A.M. (1999). The DNA double-strand break repair gene hMRE11 is mutated in individuals with an ataxia-telangiectasia-like disorder. Cell *99*, 577–587.

Strauch, K., Fimmers, R., Kurz, T., Deichmann, K.A., Wienker, T.F., and Baur, M.P. (2000). Parametric and nonparametric multipoint linkage analysis with imprinting and two-locus-trait models: application to mite sensitization. Am. J. Hum. Genet. *66*, 1945–1957.

Szczerbal, I., and Bridger, J.M. (2010). Association of adipogenic genes with SC-35 domains during porcine adipogenesis. Chromosome Res. *18*, 887–895.

Valente, E.M., Silhavy, J.L., Brancati, F., Barrano, G., Krishnaswami, S.R., Castori, M., Lancaster, M.A., Boltshauser, E., Boccone, L., Al-Gazali, L., et al; International Joubert Syndrome Related Disorders Study Group. (2006). Mutations in CEP290, which encodes a centrosomal protein, cause pleiotropic forms of Joubert syndrome. Nat. Genet. *38*, 623–625.

Xiao, R., Sun, Y., Ding, J.H., Lin, S., Rose, D.W., Rosenfeld, M.G., Fu, X.D., and Li, X. (2007). Splicing regulator SC35 is essential for genomic stability and cell proliferation during mammalian organogenesis. Mol. Cell. Biol. *27*, 5393–5402.

Yu, J., Carroll, T.J., Rajagopal, J., Kobayashi, A., Ren, Q., and McMahon, A.P. (2009). A Wnt7b-dependent pathway regulates the orientation of epithelial cell division and establishes the cortico-medullary axis of the mammalian kidney. Development *136*, 161–171.

EXTENDED EXPERIMENTAL PROCEDURES

Whole-Exome Sequencing

Whole-Exome Capture

Exome enrichment was conducted largely following the manufacturer's protocol for the NimbleGen SeqCap EZ Exome v2 (Roche NimbleGen, version 2). Briefly, three micrograms of genomic DNA was fragmented by sonication using the Covaris S2 system to achieve a uniform distribution of fragments with a mean size of 300 bp. The sonicated DNA was purified using AMPure XP Solid Phase Reversible Immobilization paramagnetic (SPRI) beads (Agencourt) followed by polishing of the DNA ends by removing the 3′ overhangs and filling in the 5′ overhangs resulting from sonication using T4 DNA polymerase and Klenow fragment (New England Biolabs). Following end polishing, a single 'A'-base was added to the 3′ end of the DNA fragments using Klenow fragment (3′ to 5′ exo minus). This prepares the DNA fragments for ligation to specialized adaptors that have a 'T'-base overhang at their 3′ends. The end-repaired DNA with a single 'A'-base overhang was ligated to paired-end adaptors (Illumina) in a standard ligation reaction using T4 DNA ligase and 2–4 μM final adaptor concentration, depending on the DNA yield following purification after the addition of the 'A'-base (a 10-fold molar excess of adaptors is used in each reaction). Following ligation, the samples were purified using SPRI beads, amplified by six cycles of PCR to maintain complexity and avoid bias due to amplification and quality controlled by library size assessment on the Agilent Bioanalyzer and quantitation using PicoGreen reagent (Invitrogen).

One microgram of amplified, purified DNA (DNA library) was prepared for hybridization by adding COT1 DNA and blocking oligonucleotides to the DNA library, desiccating the DNA completely and resuspending the material in NimbleGen hybridization buffer. The resuspended material was denatured at 95°C prior to addition of the exome capture library bait material. The DNA library and biotin-labeled capture library were hybridized by incubation at 47°C for 68 hr. Following hybridization, streptavidin coated magnetic beads were used to purify the DNA:DNA hybrids formed between the capture library and sequencing library during hybridization. The purified sequencing library was amplified directly from the purification beads using 8 cycles of PCR using Pfx DNA polymerase (Invitrogen). The libraries were purified following amplification and the library size was assessed using the Agilent Bioanalyzer. A single peak between 350-400 bp indicates a properly constructed and amplified library ready for sequencing. Final quantitation of the library was performed using the Kapa Biosciences Real-time PCR assay and appropriate amounts loaded onto the Illumina flowcell for sequencing by paired-end 50 nt sequencing on the Illumina HiSeq2000 sequencer.

Sequencing

Sequencing was performed largely as described in (Bentley et al., 2008). Following dilution to 10 nM final concentration based on the real-time PCR and bioanalyzer results, the final library stock is then used in paired-end (PE) cluster generation at a final concentration of 6-8 pM to achieve a cluster density of 600,000/mm^2 (on the Illumina HiSeq2000 instrument, v2.5 reagents). Following cluster generation, 100nt paired-end sequencing was performed using the standard Illumina protocols. Sequencing each sample in a single lane at paired-end 100 nt conditions on the Illumina HiSeq (v2.5 reagents) generated an average of 19.1Gb of pass-filter sequence data with 94.96% aligning to the genome. This amount of sequence corresponded to an average coverage of 181x over the 44 Mb of capture region. 80.41% of sequencing reads fell with 200 bp of the target region. 98.39% of the capture region was sequenced to a depth of at least 1x, 95.6% to at least 8x, 92.17% to at least 20x, and 89.42% to at least 30x.

Data Analysis

Raw sequencing data for each individual were mapped to the human reference genome (build hg19) using the Burrows-Wheeler Aligner (BWA v0.5.81536)14. The BWA aligned sequencing reads were processed by Picard (http://picard.sourceforge.net/) to label the PCR duplicates. The Genome Analysis Toolkit (GATK, version 5091) was then used to remove duplicates, perform local realignment and map quality score recalibration to produce a ''cleaned'' BAM file for each individual. SNP calls were made by the Unified Genotyper module in GATK using the ''cleaned'' BAM files in batch fashion (90 samples per batch). The resulting Variant Call Format (VCF, version 4.0) files were annotated using the GenomicAnnotator module in GATK to identify and label the called variants that are within the targeted coding regions and overlap with known and likely benign SNPs reported in dbSNP v132 (ftp://ftp.ncbi.nlm.nih.gov/snp/organisms/human_9606/VCF/v4.0/00-All.vcf.gz) with allele frequencies > 5%. The annotated VCF files were then filtered using the GATK variant filter module with a hard filter setting and a custom script for initial filtering. Variant calls that failed to pass the following filters were eliminated from the call set: (1) MQ0 > = 4 && ((MQ0 / (1.0 * DP)) > 0.1); (2) QUAL < 30.0 || QD < 5.0 || HRun > 5 || SB > 0.00; (3) Cluster size 10; (4) not contain dbSNP id; (5) inside the targeted regions. Combined VCF files were then split into individual files and remaining variants were tested for recessive segregation in the respective families. Topline statistics on 32 whole human exomes that we evaluated, which include the exomes that we evaluated in this paper, are available from the authors (unpublished data).

For each of the three families with mutation of *MRE11*, *ZNF423* or *CEP164* there was only one gene in each family in any of the homozygous regions for which the homozygous variant passed Polyphen 1 and 2 scores, segregated within the family, and was absent from >270 controls, thus validating the pathogenic relevance of the mutation (unpublished data).

CEP164 Mutation Analysis

We performed exon-PCR and Sanger sequencing of all 31 coding exons for one affected individual in each of 856 different NPHP-RC families. The number of families examined (by increasing number of organs involved) was: isolated nephronophthisis (5), isolated retinal degeneration (100), Senior-Loken syndrome (168), Joubert syndrome (240), Bardet-Biedl syndrome (195), Meckel syndrome

(52), and other severe unsolved NPHP-RC cases (96). We also examined 480 individuals from additional NPHP-RC families using massively-parallel sequencing of exon-PCR from pooled DNA samples (Otto et al., 2010).

Yeast-Two-Hybrid Screening with ZNF423

A subclone of human CEP290 was prepared using high fidelity *Taq* polymerase, spanning 1770 bp, (562 amino acids, 1917-2479) and including wild-type stop codon and cloned into pENTR-TOPO as previously described in (Sayer et al., 2006) (clone named 'JAS2'). The CEP290 subclone insert was switched to destination vector pDEST32 (binding domain containing yeast-2-hydrid vector, ''bait'') (Invitrogen). CEP290 (JAS2) was used as bait, fused to the *GAL4* DNA binding domain in the pDEST32 vector, and a human fetal brain expression library was screened and cloned into pEXPAD22 *GAL4* activation domain fusion vector (Invitrogen). Approximately 1×10^6 clones were screened after cotransforming plasmids into competent MaV203 yeast cells (lithium acetate method) and plating onto His, Leu and Trp deficient medium containing 25 mM 3-aminotriazole. Colonies were replica plated on restrictive media and surviving colonies were used for cDNA extraction. Five ml cultures were grown at 30°C overnight. cDNA was extracted using RPM yeast plasmid isolation kit™ (Bio 101 systems). cDNA was transformed into *E. coli*, purified and directly sequenced using vector specific primers. Sequence analysis allowed prediction of amino acid sequences (ORF Finder), which were then identified by BLAT analysis (http://genome.ucsc.edu). Direct yeast-2-hybrid interaction experiments allowed colony growth to be compared to 2 negative controls (respective plasmids without insert, data not shown) and 5 positive control yeast strains for different interaction strength.

Coimmunoprecipitation with ZNF423

Full length human *ZNF423* was subcloned into pcDNA3.1-NT-GFP using long range PCR (Expand, Roche) and IMAGE clone 100072717 as template. Clones were sequenced to confirm orientation and fidelity. A partial length human *CEP290* cDNA spanning 1770 bp as described above (JAS2) was subcloned into a DEST-V5 vector. HEK293 cells were transiently cotransfected with full length GFP-*ZNF423* and partial length *CEP290*-V5 using Lipofectamine 2000. After 24 hr cells were washed in phosphate-buffered saline (PBS), pelleted, and lysed in NP-40 buffer (150 mM sodium chloride, 0.5% NP-40, 50 mM Tris pH 7.4, phenylmethanesulphonylfluoride, and protease inhibitors). The lysate was centrifuged for 20 min at 10,000 *g* at 4°C and the supernatant was precleared with protein G sepharose beads (GE Healthcare, Giles, Buckinghamshire, UK). After removal of protein G the supernatant was then incubated overnight with protein G and 1 μg of either anti-V5 (Invitrogen) or mouse IgG (Sigma) at 4°C. The beads were washed extensively in lysis buffer and bound proteins resolved by 10% SDS-polyacrylamide gel electrophoresis as described above. GFP-tagged proteins were detected with anti-GFP-conjugated to HRP (Santa Cruz) 1:5,000 and V5-tagged proteins were detected with anti-V5 conjugated to HRP (Invitrogen) 1:5,000.

Spheroid Assays

IMCD3 Cell Culture

IMCD3 is a mouse inner medullary collecting duct cell line. The cells were cultured in Dulbecco's Modified Eagle's Medium (DMEM):F12 (1:1) (GlutaMAX, GIBCO), supplemented with 10% Fetal Calf Serum (FCS) and penicillin and streptomycin (1% P/S). Cells were incubated at 37°C in 5% carbon dioxide (CO_2) to approximately 90% confluence.

Transfections

Before exposing the cells to different experimental conditions, cells were seeded in 6-, 24- or 48-well plates, depending on the experimental setup. After at least 6 hr, the cells were transfected with Lipofectamine RNAimax (Invitrogen, 13778-075), according to the supplier's protocol. Opti-MEM (Invitrogen, 31985-062) was used to dilute the ON-TARGETplus siRNA SMARTpools (Thermo Scientific Dharmacon) for Nontargeting pool (D-001810-10) or Cep164 (L-057068-01).

IMCD3 Spheroid Growth Assay

Cells were trypsinized 24 hr post-transfection and resuspended cells were then mixed 1:1 with growth factor-depleted matrigel (BD Bioscience). After the matrigel polymerized for 20 min at 37°C, warm medium was dropped over the matrix until just covered. The IMCD3 cells formed spheroids with cleared lumens 3 days later. Medium was removed by pipetting and the gels were washed three times for 10 min with warm PBS supplemented with calcium and magnesium. The gels were then fixed in fresh 4% PFA for 30 min RT. After washing three times in PBS after fixation, the cells were permeabilized for 15 min in gelatin dissolved in warm PBS (350 mg/50 mL) and 0.5% Triton X-100. Primary antibody (mouse anti-acetylated tubulin, Sigma, at 1:20,000) was diluted in the permeabilization gelatin buffer and incubated at 4°C overnight. After washing the spheroids 3 times for 30 min in permeabilization buffer, goat anti-mouse Alexa-555 secondary antibody (Invitrogen) was diluted 1:500 in permeabilization buffer and incubated overnight at 4°C. The next day, spheroids were washed 3 times in permeabilization buffer and mounted with Dapi (1:2,000) in Fluoromount-G (Cell Lab, Beckman Coulter). Images were taken with a Zeiss LSM510 confocal microscope and 50 spheroids per condition were scored. GraphPad Prism 5.0 was used to perform two-tailed Student's t tests.

RT-qPCR for Cep164

IMCD3 cells were transfected with nontargeting siControl or si*Cep164* oligonucleotides (Dharmacon, ON-TARGETplus SMARTpool *Cep164*) using Lipofectamine RNAimax (Invitrogen) in 6 well plates seeded with cells at 50% confluency. Cells were lysed 24, 48 and 72 hr after transfection and total RNA was isolated (RNeasy Mini Kit, QIAGEN, 74106) and measured (NanoDrop spectrophotometer ND-1000, Thermo Fischer Scientific Inc.). cDNA was synthesized from 500 ng RNA template using the iScript cDNA Synthesis Kit (Bio-Rad, 170-8891) according to the supplier's protocol. Dilutions were made for RT-QPCR analysis to determine the expression of Cep164, normalized against reference gene RPL27. The primers (Sigma) used are mCep164 forward 5′-AGAGTGACAACCA

GAGTGTCC, mCep164 reverse 5′-GGAGACTCCTCGTACTCAAAGTT, mRPL27 forward 5′- CGCCCTCCTTTCCTTTCTGC and mRPL27 reverse 5′-GGTGCCATCGTCAATGTTCTTC. The iQ SYBR Green Supermix (Bio-Rad, 170-8880) was used to multiply and measure the cDNA with a CFX96 Touch Real-Time PCR Detection System (Bio-Rad). All samples were run in triplicate in 20 μl reactions. The following PCR program was used: 95°C for 3 min, followed by 40 cycles of 10 s at 95°C, 30 s at 51.5/61°C and 30 s at 72°C, then 10 s at 95°C followed by a melt of the product from 65°C-95°C.The ΔΔCT method was used for statistical analysis to determine gene expression levels.

Immunofluorescence and Confocal Microscopy

For immunostaining IMCD3 cells, cells were grown on coverslips and fixed for 30 min in 4%PFA followed by a 15 min permeabilization step in 0.5%Triton X-100/1%BSA/PBS. Primary antibody incubations (human anti-CREST at 1:1,000, mouse anti-acetylated tubulin at 1:20,000) were performed overnight in 1% BSA/PBS. Secondary antibody incubations were performed for 1 hr at RT. DAPI incubations were performed for 10 min at RT. Coverslips were mounted in Fluoromount G (Cell Lab, Beckman Coulter). Confocal imaging was performed using Zeiss LSM510 Confocal laser microscope and images were processed with the LSM software. Approximately 250 events per condition were scored. GraphPad Prism 5.0 was used to perform two-tailed Student's t tests.

Cell-Cycle Studies

Generation of IMCD3 and hTERT-RPE Cell Lines that Are Doxycycline-Inducible for N-GFP-CEP164 Constructs

Both, IMCD3 and hTERT-RPE cells were stably transfected with N terminally GFP tagged human *CEP164* constructs in a retroviral vector for doxycycline (Dox)-inducible expression (pRetroX-Tight-Pur). Following selection on puromycin for 2 weeks, cells were induced with 10 ng/ml of doxycyclin for 20 hr. Based on the GFP expression levels upon immunofluorescence, clonal cells were generated for IMCD3 cells.

Cell-Cycle Studies

IMCD3 cells Dox-inducible for human N-GFP-Cep164-WT (wild-type) or N-GFP-Cep164-Q525X (mutant) were transfected with either nontargeting control siRNA (50 nM, Dharmacon D-001206-14-20) or mouse *Cep164* siRNA (50 nM, Smartpool Dharmacon L-057068-01-0020) using Polyplus transfection reagents. Cells were then re-plated and treated for double thymidine (2 mM) blocks beginning at 24 hr post transfection. At the same time, cells were also induced with doxycycline (10 ng/ml) for *N-GFP-Cep164-WT* or *N-GFP-Cep164-Q525X*. Cells were released from second thymidine block for 6 hr and fixed with 2% PFA and stained with PI/RNase staining solution (BD Biosciences). FACS analysis for cell-cycle histograms was performed and data were then analyzed using Modfit software. Mean and SD of % DNA amount for different phases (triplicate samples) were calculated and plotted as bar diagram.

Cell-Proliferation Studies

IMCD3 cells Dox-inducibly expressing human *N-GFP-CEP164-WT* or *N-GFP-CEP164-Q525X* were transfected with either nontargeting control siRNA (50 nM, Dharmacon D-001206-14-20) or mouse *Cep164* siRNA (50 nM, Smartpool Dharmacon L-057068-01-0020) using Polyplus transfection reagents. Cells were then re-plated in triplicate of 10,000 cells for each group and treated for thymidine (2 mM) blocks beginning at 24 hr post transfection. At the same time, cells were also induced with doxycycline (10 ng/ml) for *N-GFP-CEP164-WT* or *N-GFP-CEP164-Q525X* expression. Cells were counted at 48, 72, and 96 hr post transfection.

Roscovitine Studies

Cell Culture and Cell Irradiation

Sh-Neg-IMCD3 cells were maintained in DMEM:F12 supplemented with 10% FCS, 1% Penicillin/Streptomycin and 5 μg/ml Puromycin (all from GIBCO/Invitrogen, Carlsbad, CA) and maintained in a 5% CO_2 humidified atmosphere at 37°C. Roscovitine (Chem Partners, China) was incubated at 80 μM for 24 hr. Ultraviolet (UV) irradiation was performed using a UV Stratalinker™ (Stratagene/Agilent, Santa Clara, CA) at 30 J/m^2 dose; cells were left to recover for 1 hr at 37°C before further analyses.

Immunoblotting, Immunofluorescence, and Subcellular Fractionation

Cells were lysed as previously described (Bukanov et al., 2006). Subcellular fractionation was performed using Nuclear Extract Kit according to the manufacturer's instructions (Active Motif, Carlsbad, CA). Protein concentration was determined by BCA protein assay (Pierce/Thermofisher, Rockford, IL). Proteins were resolved on SDS PAGE 5%–12% gradient and transferred using iBlot system (Invitrogen). The following antibodies were used: CEP164 (Novus Biologicals, Littleton, CO), Phospho-Chk1 (Ser317) and phospho-H2AX (Ser139) (Cell Signaling, Danvers, MA), Chk1 (Upstate/Millipore, Billerica, MA), H2AX and 13.3.3 (AbCam, Cambridge, MA) and Sam-68 (Santa Cruz Biotech. Santa Cruz, CA). Primary antibodies were detected with anti-rabbit or anti-mouse horseradish peroxidase-conjugated secondary antibodies (Promega, Madison, WI) and revealed by ECL (Amersham, Little Chalfont, Buckinghamshire, UK) as previously described (Bukanov et al., 2006). For immunofluorescence, cells were fixed for 20 min in 4% paraformaldehyde (Electron Microscopy Science, Hatfield, PA) in PBS (pH 7.2) and were permeabilized with 0.1% Triton X-100 in PBS. Immunofluorescence was then performed as previously described (Smith et al., 2006).

Gene Expression Analysis

Gene expression analysis was performed as described before (Smith et al., 2006, 17-pp2821-2831) using TAQ-Man gene expression assays (Applied Biosystems/Invitrogen, Carslbad, CA).

Interaction Studies of CEP164 with TTBK2 and CCDC92

Yeast Two-Hybrid

A GAL4-based yeast two-hybrid system was used to screen for binary CEP164 interactors by using methods described by Letteboer and Roepman (Letteboer and Roepman, 2008). Bait constructs expressing full length CEP164 ($CEP164^{fl}$) and several fragments thereof ($CEP164^{1-550}$, $CEP164^{551-1100}$ and $CEP164^{1101-1460}$) were used to screen two retinal cDNA libraries: a bovine library of randomly primed retina cDNA and a human library of oligo-dT primed retina cDNA (Letteboer and Roepman, 2008).

GST Pull-Down

Full length 3xFlag-CCDC92 and 3xFlag-TTBK2 were expressed in COS-1 cells. $CEP164^{fl}$, $CEP164^{1-550}$, $CEP164^{551-1100}$ and $CEP164^{1101-1640}$ were cloned in pDEST15 and the resulting expression constructs were transformed in BL21DE3 to express glutathione S-transerase (GST) fusion proteins. The GST pull-down was performed as described by Coene et al. (Coene et al., 2011). The results were assessed by immunoblotting, and Flag-tagged proteins were detected using anti-Flag primary antibodies (Sigma-Aldrich) and goat-anti-mouse IRDye800 secondary antibodies (Rockland, Immunochemicals, Gilbertsville, PA, USA). A Li-Cor Odyssey 2.1 scanner was used for imaging.

Coimmunoprecipitation

3xHA-$CEP164^{fl}$ was expressed in combination with either 3xFlag-$CCDC92^{fl}$ or 3xFlag-$TTBK2^{fl}$ in COS-1 cells (and vice versa with swapped tags). 3xFlag-dNp63 or 3xHA-dNp63 was used as a control for specificity. The coimmunoprecipitation was performed as described by Coene et al. Transfected COS-1 cells were lysed and incubated with α-M2-agarose from mouse (Sigma-Aldrich) or α-HA affinity matrix from rat (Roche) for 2 hr at 4°C. After washing, sample buffer was added to the beads and the sample was heated. Beads were then precipitated by centrifugation and the supernatant was analyzed by immunoblotting to assess if TTKB2 and CCDC92 indeed coimmunoprecipitated with CEP164.

Interaction Studies of CEP164 with DVL3

Immunoprecipitation Coupled to Mass Spectrometry

Mouse embryonal fibroblasts were grown in DMEM supplemented with 10% fetal bovine serum at 37°C to confluency and cell pellets are frozen at −80°C. Cells were then lysed in lysis buffer (0.5% NP40; 150mM NaCl; 50 mM Tris pH 7.4) and subjected to immunoprecipitation with antibodies against Dvl3 (sc-8027); Dvl2 (sc-8026) or control IgG (sc-2025; Santa Cruz Biotechnology). Proteomics grade trypsin (Sigma) was added to the beads directly (10 ng/μl) and left at 37°C for 12 hr. Tryptic digested peptides were desalted using ZipTip C18 column (Millipore) based on the manufacturer's protocol. LC-MS/MS was performed on a NanoAcquity UPLC (Waters) on-line coupled to an ESI Q-TOF Premier (Waters) mass spectrometer. Trypsin digested peptides eluted from ZipTip column were diluted in autoclaved M.Q. water (Millipore) and loaded onto a 180 μm x 20 mm nanoAcquity UPLC Symmetry trap column (Waters) packed with 5 μm BEH C-18 beads. After 1 min of trapping, peptides were eluted through a 75 μm x 150 mm nanoAcquity (Waters) analytical column packed with 1.7 μm BEH C-18 beads at a flow rate of 400 nL/min using a gradient of 3 – 40% acetonitril with 0.1% formic acid for 35 min at a temperature of 35°C. Effluent was directly fed into the ESI source of the mass spectrometer. Raw data was acquired in data independent MS^E Identity (Waters) mode. Precursor ion spectra were acquired with collision energy 5 V and fragment ion spectra with a collision energy 20-35 V ramp in alternating 1 s scans. Raw data was then subjected to a database search using species specific Uniprot and NCBI mouse protein database by the PLGS2.3 software (Waters). Acetyl N-terminal, Deamidation N and Q, Carbamidomethyl C and Oxidation M were set as variable modifications. Peptide accuracy and MS/MS fragment mass accuracy was less than 20 ppm.

Western Blotting and Immunoprecipitation

Immunoblotting and sample preparations were performed as previously described (Bryja et al., 2007b). HEK293 cells were transfected with the indicated constructs and lysed 48 hr later. Samples were analyzed using SDS-PAGE and Western blotting, or subjected to immunoprecipitation. The antibodies used include the following: Dvl3 (sc-8027), Dvl2 (sc-8026), mouse IgG (sc-2025), from Santa Cruz Biotech, CEP164 (4533.00.02) from Sdix, HA.11 (MMS-101P) from Covance, GFP (3H9), RFP (3F5) from Chromotek and FLAG M2 (F1804), GST (G1160) from Sigma.

Immunoprecipitation was performed as previously described (Bryja et al., 2007a). The antibodies used for immunoprecipitation were RFP Trap from Chromotek, HA.11 (MMS-101P) from Covance, anti FLAG (F1804; Sigma), anti Dvl3 (sc-8027), anti Dvl2 (sc-8026) (all Santa Cruz Biotechnology).

GST Pull-Down

Production of recombinant GST-tagged fragments of CEP164 (Sivasubramaniam et al., 2008) was induced by adding 0.2 mM IPTG and grown for 4 hr at 37°C. The bacteria were spun down at 4000 g/4°C/10 min and the pellet was resuspended in 10 ml of GST lysis buffer (50 mM Tris-Cl pH 7.5, 150 mM NaCl, 5mM $MgCl_2$, protease inhibitors (Roche)) and stored at −80°C. Then the solution was thawed, sonicated for 3x30 s and spun down 15000 g/4°C/15 min. The supernatant was then used for incubation with GST beads for 2 hr at rotator (100 μl of beads per 100 ml of original bacterial culture). After incubation beads were washed 3 times with 1 ml of GST lysis buffer and frozen at −80°C as 25% slurry in GST lysis buffer +20% glycerol.

HEK293T cells were transfected according to the scheme, grown for 24 or 48 hr and lysed in 0.5% NP 40 lysis buffer (0.5% NP40, 50 mM Tris pH 7.4, 1 mM EDTA, 150 mM NaCl) with added protease inhibitors (Roche) and phosphatase inhibitors (Calbiochem). The lysate was spun down at 16100 g/4°C/10 min and the supernatant was used for overnight incubation with 15 μl of solid GST beads containing GST recombinant proteins on the rotator. After the incubation samples were washed with 800 μl 0.5% NP 40 lysis buffer,

the GST beads were collected at 0.1 g/4°C/1 min, the supernatant was aspirated out and this washing was repeated 6 times. Proteins were eluted with 45 μl of 2x Laemmli buffer.

Immunohistochemistry

HEK293 cells were seeded at approx. $2x10^5$ cells/well on collagen coated coverslips in 24-well plates. Cells were fixed in fresh 4% paraformaldehyde, permeabilized with 0.05% Triton X-100, blocked with PBTA (3% BSA, 0,25% Triton, 0,01% NaN_3) for 1 hr and incubated overnight with primary antibodies CEP164 (4533.00.02) from Sdix and Dvl2 (sc-8026 from Santa Cruz Biotechnology). Next day, coverslips were washed in PBS, and incubated with secondary antibodies: Alexa 488, Alexa 568 (Invitrogen), washed with PBS, stained with DAPI (1:5000) and mounted on coverslips. Cells were visualized using a Leica TCS SP-5 confocal microscope.

Multicolor Competition Assay

MCA was performed as described previously (Smogorzewska et al., 2007). Briefly, 1.7×10^5 U2OS-GFP were reverse transfected with 64 pmol siRNA duplex using Lipofectamine RNAiMAX (Invitrogen) as per manufactures instructions. 48 hr post transfection siRNA treated U2OS-GFP were mixed with anti-Luciferase siRNA treated U2OS-RFP cells at a 1:1 ratio. 72 hr post transfection cells were treated with DNA damaging agents as depicted. Cells were harvested for FACS analysis 7 days post treatment. siRNA duplex sequences were as follows: Luc: CGTACGCGGAATACTTCGA (siRNA targeting firefly luciferase mRNA), CEP164#1: GGACCATC CATGTGACGAA; CEP164#2: GGCTGGAACGTGTCAAGAA; CEP164#3: GAGTTGGAGTCTCAACAGA; ZNF423#1: GGAGAACCA CAAGAACATT; ZNF423#2: CGAGTGCAGTGTCAAGTTT; ZNF423#3: GCATCAACCACGAGTGTAA, all from Ambion; BRCA2: (Stealth siRNA, Invitrogen) used as a combination of three siRNAs: GGAACCAAATGATACTGATCCATTA, GGAGGACTCCTTATGTC CAAATTTA, GAGCGCAAATATATCTGAAACTTC;ATM (Stealth siRNA, Invitrogen) used as a combination of three siRNAs: GCGCA GTGTAGCTACTTCTTCTATT, GGGCCTTTGTTCTTCGAGACGTTAT, GCAACATTTGCCTATATCAGCAATT; anti-CEP164 antibody for immunoblot was from Novus (cat #45330002).

Quantitative RT-PCR

Intron spanning primer pairs were designed for quantitative RT-PCR of *ZNF423* and *beta-actin* as control. RNA was extracted from the siRNA treated U2OS cells using QIAGEN RNeasy Plus Mini Kit. First-strand cDNAs were then synthesized using the Invitrogen SuperScript III Reverse Transcriptase kit. Quantitative RT-PCR was performed using Platinum SybrGreen Super Mix (Invitrogen) according to the manufacturer's instructions. Sequences of primer pairs were: *Beta-actin* forward: GCTACGAGCTGCCTGACG, *Beta-actin* reverse: GGCTGGAAGAGTGCCTCA, *ZNF423* forward: GTCTCTGGCAGACCTGACG, *ZNF423* reverse: AGAGTTGTGGG TCGTCATCA.

ZNF423 DNA Damage Response

Lentivirus constructs were obtained in a pLKO vector (Sigma) modified to express Emerald GFP in place of the Puromycin marker. Transduction efficiencies were ~70% by GFP fluorescence. For DDR assays, transduced cells were plated at $1x10^5$ per well in 12-well plate containing poly-L-lysine coated glass cover slides one day before irradiation with a calibrated source (Moores UCSD Cancer Center). Two hr after irradiation, cells were fixed with 4% PFA. Mouse anti-γH2AX (Upstate, clone JBW30) and rabbit anti-ZNF423 (Y-W Cho and B.A.H. unpublished data) antibodies were added at room temperature for 2 hr. Donkey anti-mouse (Alexa fluor 555) and anti-rabbit (Alexa fluor 488) antibodies (Jackson Immunoresearch) were incubated at room temperature for 1 hr. Images were captured on an Olympus FV1000 confocal microscope. Signal intensities of γH2AX were quantified from image files in ImageJ software. Distribution of foci in *Zfp423*-knockdown cells did not meet the conditions of a t test and were analyzed by the Mann-Whitney U (Wilcoxon rank sum) test implemented in R 2.8.1.

FACS Analysis of γH2AX

Both control and *Cep164* stable knockdown IMCD3 cells were irradiated with indicated doses (Figure 6Q). Cells were then fixed 60 min post-irradiation with 2% paraformaldehyde, permeabilized with 0.1% SDS and stained with rabbit γH2AX (Cell Signaling). Alexa-fluor-488 conjugated secondary anti-rabbit antibody was used to analyze the mean fluorescent intensity (MFI) of samples in triplicate in the FACS facility (Cancer Center, University of Michigan). Results shown are representation of mean and SD of triplicate samples.

Statistical Analysis

Student's two-tailed nonpaired t tests and normal distribution two-tailed z tests were carried out using pooled standard error and s.d. values to determine the statistical significance of different cohorts.

SUPPLEMENTAL REFERENCES

Bentley, D.R., Balasubramanian, S., Swerdlow, H.P., Smith, G.P., Milton, J., Brown, C.G., Hall, K.P., Evers, D.J., Barnes, C.L., Bignell, H.R., et al. (2008). Accurate whole human genome sequencing using reversible terminator chemistry. Nature *456*, 53–59.

Bryja, V., Gradl, D., Schambony, A., Arenas, E., and Schulte, G. (2007a). Beta-arrestin is a necessary component of Wnt/beta-catenin signaling in vitro and in vivo. Proc. Natl. Acad. Sci. USA *104*, 6690–6695.

Bryja, V., Schulte, G., Rawal, N., Grahn, A., and Arenas, E. (2007b). Wnt-5a induces Dishevelled phosphorylation and dopaminergic differentiation via a CK1-dependent mechanism. J. Cell Sci. *120*, 586–595.

Bukanov, N.O., Smith, L.A., Klinger, K.W., Ledbetter, S.R., and Ibraghimov-Beskrovnaya, O. (2006). Long-lasting arrest of murine polycystic kidney disease with CDK inhibitor roscovitine. Nature *444*, 949–952.

Coene, K.L., Mans, D.A., Boldt, K., Gloeckner, C.J., van Reeuwijk, J., Bolat, E., Roosing, S., Letteboer, S.J., Peters, T.A., Cremers, F.P., et al. (2011). The ciliopathy-associated protein homologs RPGRIP1 and RPGRIP1L are linked to cilium integrity through interaction with Nek4 serine/threonine kinase. Hum. Mol. Genet. *20*, 3592–3605.

Giorgio, G., Alfieri, M., Prattichizzo, C., Zullo, A., Cairo, S., and Franco, B. (2007). Functional characterization of the OFD1 protein reveals a nuclear localization and physical interaction with subunits of a chromatin remodeling complex. Mol. Biol. Cell *18*, 4397–4404.

Habbig, S., Bartram, M.P., Müller, R.U., Schwarz, R., Andriopoulos, N., Chen, S., Sägmüller, J.G., Hoehne, M., Burst, V., Liebau, M.C., et al. (2011). NPHP4, a cilia-associated protein, negatively regulates the Hippo pathway. J. Cell Biol. *193*, 633–642.

Letteboer, S.J., and Roepman, R. (2008). Versatile screening for binary protein-protein interactions by yeast two-hybrid mating. Methods Mol. Biol. *484*, 145–159.

Liebau, M.C., Höpker, K., Müller, R.U., Schmedding, I., Zank, S., Schairer, B., Fabretti, F., Höhne, M., Bartram, M.P., Dafinger, C., et al. (2011). Nephrocystin-4 regulates Pyk2-induced tyrosine phosphorylation of nephrocystin-1 to control targeting to monocilia. J. Biol. Chem. *286*, 14237–14245.

Otto, E.A., Schermer, B., Obara, T., O'Toole, J.F., Hiller, K.S., Mueller, A.M., Ruf, R.G., Hoefele, J., Beekmann, F., Landau, D., et al. (2003). Mutations in INVS encoding inversin cause nephronophthisis type 2, linking renal cystic disease to the function of primary cilia and left-right axis determination. Nat. Genet. *34*, 413–420.

Otto, E.A., Ramaswami, G., Janssen, S., Chaki, M., Allen, S.J., Zhou, W., Airik, R., Hurd, T.W., Ghosh, A.K., Wolf, M.T., et al.; GPN Study Group (2011). Mutation analysis of 18 nephronophthisis associated ciliopathy disease genes using a DNA pooling and next generation sequencing strategy. J. Med. Genet. *48*, 105–116.

Sayer, J.A., Otto, E.A., O'Toole, J.F., Nurnberg, G., Kennedy, M.A., Becker, C., Hennies, H.C., Helou, J., Attanasio, M., Fausett, B.V., et al. (2006). The centrosomal protein nephrocystin-6 is mutated in Joubert syndrome and activates transcription factor ATF4. Nat. Genet. *38*, 674–681.

Sivasubramaniam, S., Sun, X., Pan, Y.R., Wang, S., and Lee, E.Y. (2008). Cep164 is a mediator protein required for the maintenance of genomic stability through modulation of MDC1, RPA, and CHK1. Genes Dev. *22*, 587–600.

Smith, L.A., Bukanov, N.O., Husson, H., Russo, R.J., Barry, T.C., Taylor, A.L., Beier, D.R., and Ibraghimov-Beskrovnaya, O. (2006). Development of polycystic kidney disease in juvenile cystic kidney mice: insights into pathogenesis, ciliary abnormalities, and common features with human disease. J. Am. Soc. Nephrol. *17*, 2821–2831.

Smogorzewska, A., Matsuoka, S., Vinciguerra, P., McDonald, E.R., 3rd, Hurov, K.E., Luo, J., Ballif, B.A., Gygi, S.P., Hofmann, K., D'Andrea, A.D., and Elledge, S.J. (2007). Identification of the FANCI protein, a monoubiquitinated FANCD2 paralog required for DNA repair. Cell *129*, 289–301.

Zhou, W., Dai, J., Attanasio, M., and Hildebrandt, F. (2010). Nephrocystin-3 is required for ciliary function in zebrafish embryos. Am. J. Physiol. Renal Physiol. *299*, F55–F62.

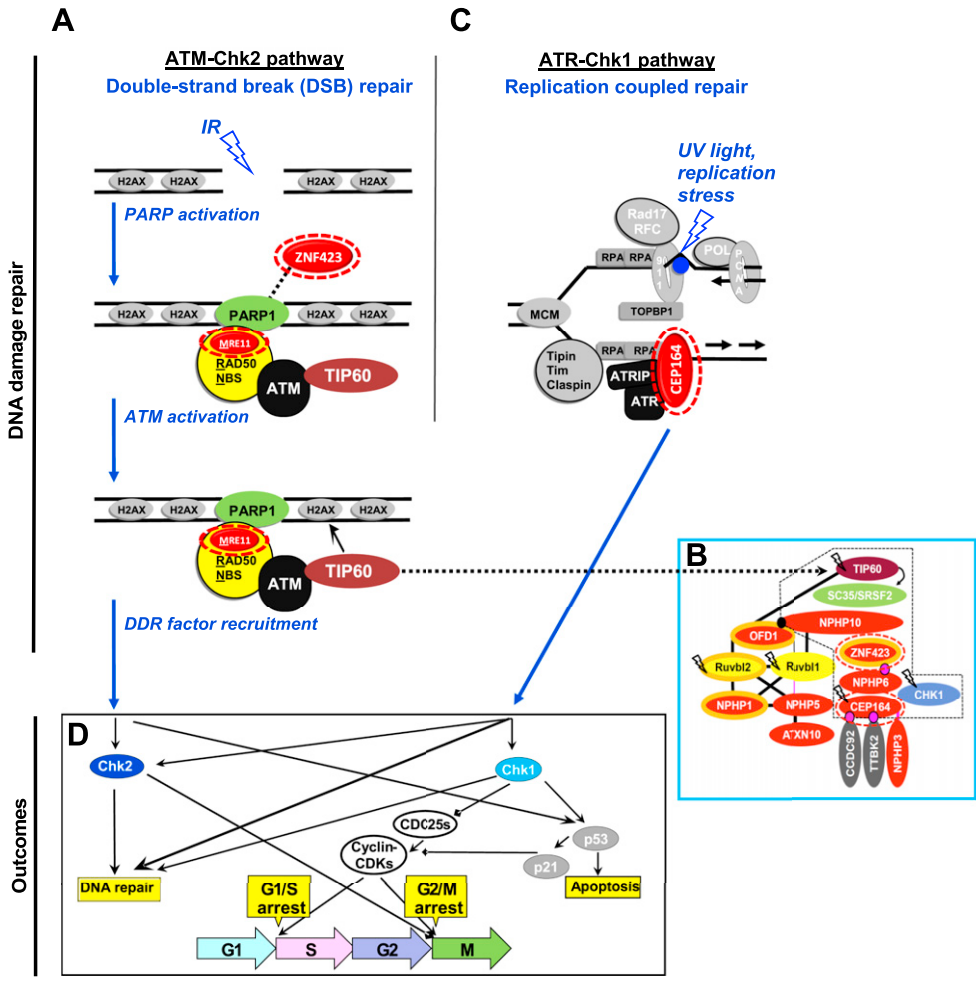

Figure S1. Links of Identified Nephronophthisis-Related Ciliopathy (NPHP-RC) Proteins to DDR Signaling and Cell-Cycle Control

DDR pathways function to sense and repair DNA damage and, if repair is incomplete, arrest cell cycle at checkpoints to avoid propagation of DNA replication errors.

Columns depict two pathways of DDR signaling, the ATM (ataxia-telangiectasia mutated) pathway (A), and the ATR (ATM-and-Rad-related) pathway (C).

Rows depict stages of DDR signaling including DNA damage sensing and repair (A, C), as well as outcomes regarding checkpoint activation, cell-cycle arrest, and apoptosis (D).

Some known components of DDR are shown in gray. Proteins relevant to this study are shown in color. Gene products identified in this study as mutated in individuals with NPHP-RC are encircled with a red dashed oval.

Each of the 3 NPHP-RC proteins that we discovered most recently, MRE11, ZNF423 and CEP164 as well as others that we discovered recently, including ATXN10 (Sang et al., 2011) and SDCCAG8/NPHP10 (Otto et al., 2010) exhibit a functional connection to DDR pathways as follows:

(A) Within the ATM-Chk2 pathway ionizing radiation (IR) can induce DNA double-strand breaks (DSB) activating PARP1. PARP1 may interact with ZNF423 (Figure 2E) (Ku et al., 2003), which we found here to be defective in individuals with NPHP-RC (Figures 1C and 1D). PARP1 recruits the MRN/ATM complex to DSBs. Activation of the ATM kinase activity by MRN (a heterotrimer of *M*RE11, *R*ad50 and *N*bs) and TIP60 leads to i) induction of the γH2AX-dependent signaling cascade, ii) phosphorylation of CHK2 and p53 and, iii) to the recruitment of a large number of other DDR factors (not shown). We here detect an *MRE11* mutation in an individual with NPHP-RC (Figures 1A and 1B). The ATM activator TIP60 is part of the 'TIP60 protein complex' (B).

(B) Relationships of TIP60 with other proteins are shown within a blue inset, including gene products that are mutated in NPHP-RC of humans (red), mouse (orange rim), and zebrafish (yellow). Indirect protein interactions are depicted as black lines, direct interaction as black dots. Protein-protein interactions identified within this study are shown as purple lines or dots. Proteins that we detected as defective in NPHP-RC in this study are encircled by a red dotted line. TIP60 activates SC35/SRSF2 (Edmond et al., 2011) and directly interacts with the NPHP-RC protein OFD1 (Giorgio et al., 2007). TIP60 colocalizes to nuclear foci with the proteins encircled by a black dashed line (see Figure 4). The proteins marked with a lightning have known functions in DDR signaling.

(C) Within the ATM-to-Chk1 pathway DNA lesions induced by UV light or replication stress (denoted by blue oval) cause replication fork stalling and accumulation of RPA-coated ssDNA regions, which recruit the ATR/ATRIP and the RAD17/RFC2-5 complexes. RAD17/RFC2-5 loads the 9-1-1 complex and stimulates ATR kinase activity by the 9-1-1-associated protein TOPBP1. ATR then activates Chk1 phosphorylation (modified from Ciccia and Elledge, 2010). CEP164 interacts with ATRIP through its N-terminal interaction domain and is phosphorylated by ATR in response to DNA damage by UV light (Sivasubramaniam et al., 2008).

(D) The DDR pathways are important to sense and repair DNA damage and, if repair is incomplete, arrest cell cycle at checkpoints. If DNA repair is successful, cell cycle progresses. If DNA repair fails, apoptosis may result or, through activation of checkpoint proteins (Chk1 and Chk2) and inhibition of the CDC25s, cell-cycle arrest in G_1/S or G_2/M may result.

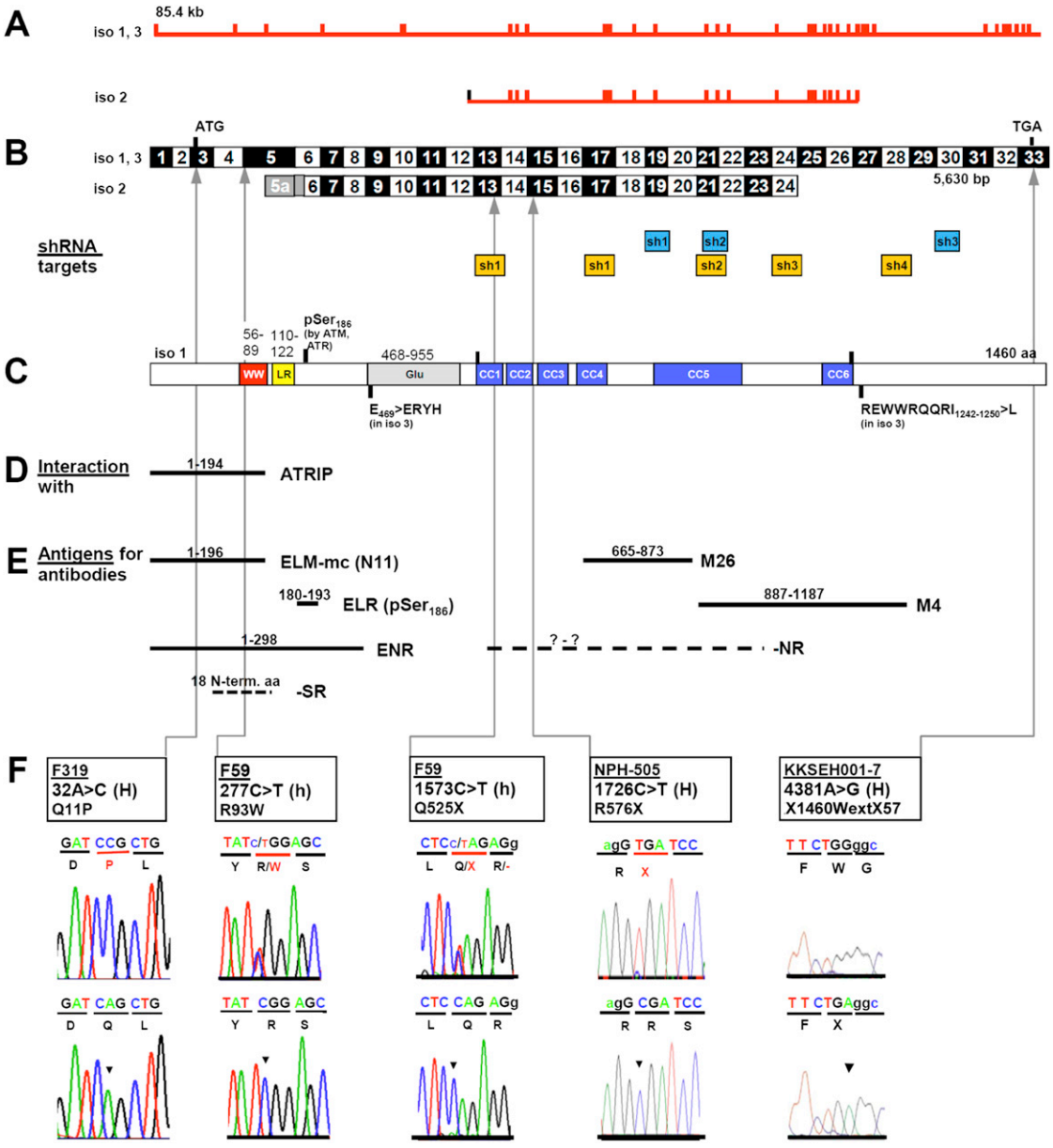

Figure S2. Alternative Transcripts, Knockdown Targets, and Human Mutations of *CEP164* with Interacting Domains, Interaction Partners, and Antigens of the Cep164 Protein

(A) The *CEP164* gene extends over 85.4 kb, contains 33 exons (vertical hatches) and an alternative exon 5a used in isoform 2.

(B) Exon structure of human *CEP164* cDNA. Positions of start codon (ATG) and of stop codon (TGA) are indicated. For the mutations detected (see (F) arrows indicate positions in relation to exons and protein domains (see (C). Positions of exon-targeting shRNAs are shown for knockdown in human (orange) and mouse (blue).

(C) Domain structure of the CEP164 protein. One N-terminal globular domain (WW), a lysine-rich repeat (LR), a glutamate-rich region (Glu), and five coiled-coil domains (CC1-5) are predicted.

(D) Minimal segment to which CEP164 binds the interaction partner ATRIP has been mapped.

(E) Extent of antigens used for α-CEP164 antibody production.

(F) *CEP164* mutations detected in 4 families with NPHP-RC. Family number and predicted translational change are indicated (see Table 1). Sequence traces are shown for mutations above normal controls. Mutated nucleotides are indicated by arrow heads in traces of normal controls. (H), homozygous mutation; (h), heterozygous mutation (see also Figure 1).

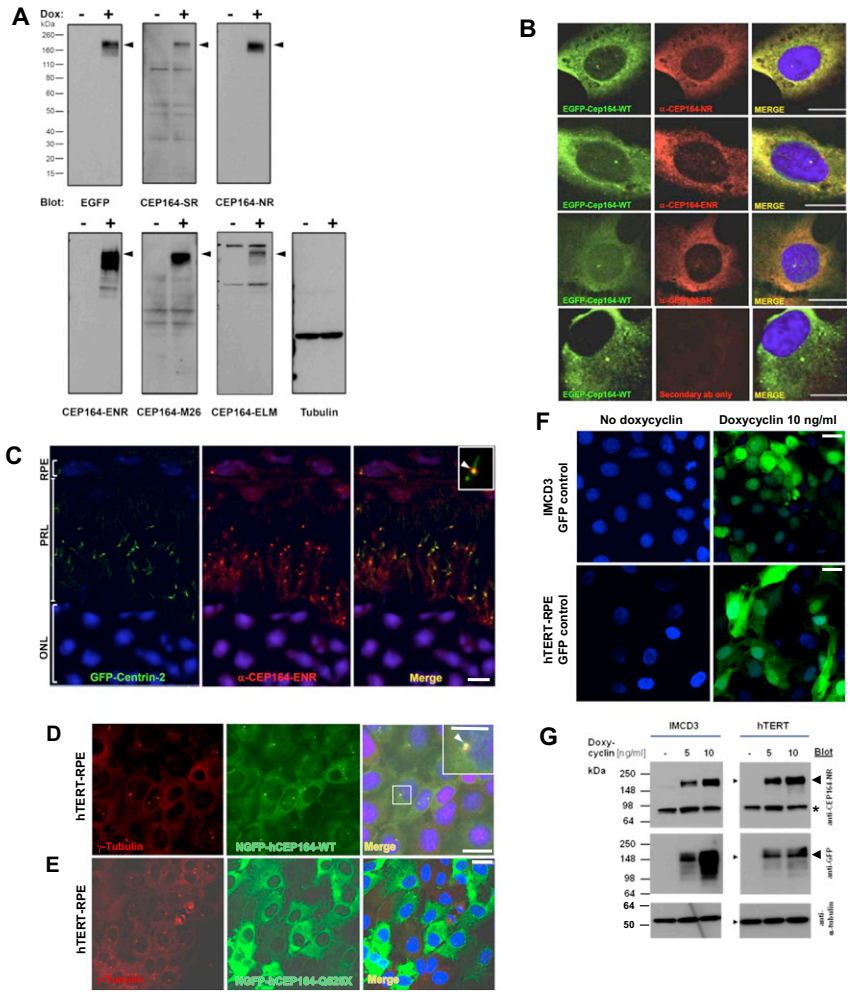

Figure S3. Subcellular Localization of CEP164

(A) Characterization of anti-CEP164 antibodies by immunoblotting. IMCD3 cells that doxycycline-inducibly express GFP-CEP164 isoform 1 were induced with (+) or without (-) 10 ng/ml doxycyclin for 20 hr. 20 μg of RIPA extracted cell lysates were subjected to SDS-PAGE and blotted with the indicated antibodies. Molecular weight is shown in kDa. Note that anti-CEP164 antibodies recognize a band compatible with the size of EGFP-CEP164 isoform 1 (191 kDa; arrow heads). Loading control (on right) uses an anti-α−tubulin antibody.

(B) Characterization of α-CEP164 antibodies by overexpression of N terminally GFP-labeled human isoform 1 wild-type construct EGFP-CEP164-WT and immunofluorescence in cell lines. Cells were costained with antibodies α-CEP164-NR, -ENR, and -SR (red), respectively, demonstrating colocalization (Merge) with N-EGFP-hCEP164-WT (green). The secondary antibody alone (lower panels) does not result in a signal. Scale bars, 5 μm.

(C) CEP164 in GFP-Centrin-2 mouse photoreceptors. In photoreceptors of centrin-2-GFP mice, immunofluorescence using anti-CEP164-ENR antibody detects Cep164 at basal bodies/mother centrioles (visible as a single red dot), whereas centrin-2-GFP is expressed at both centrioles, mother and daughter. Inset shows enlargement of a representative centrosome at 3-fold higher magnification. Nuclei are stained with DAPI. Scale bars, 5 μm. ONL, outer nuclear layer; PRL, photoreceptor layer; RPE, retinal pigment epithelium.

(D–G) Expression of mutant *CEP164* in hTERT-RPE cells abrogates localization to centrosomes. (D) Doxycyclin (Dox)-inducible overexpression of N terminally GFP-tagged human full-length CEP164 wild-type isoform 1 (NGFP-hCEP164-WT) in hTERT-RPE (human retinal pigment epithelium) cells demonstrates, in addition to a cytoplasmic expression pattern, localization at centrosomes. (E) In contrast, the signal at centrosomes is abrogated upon overexpression of an N terminally GFP-tagged truncated *CEP164* construct (NGFP-CEP164-Q525X) representing the mutation p.Q525X occurring in NPHP-RC family F59. Similar data was obtained upon CEP164 expression in IMCD3 cells (see also Figures 3B–3D). (F) Expression of GFP alone as a negative control yielded no centrosomal expression in IMCD3 or hTERT-RPE cells. hTERT-RPE cells were stably transfected with the *CEP164* constructs in a retroviral vector for doxycyclin-inducible expression (pRetroX-Tight-Pur). Following selection with puromycin for 2 weeks, cells were induced with 10 ng/ml of doxycyclin for 20 hr. Cells were then costained with γ-tubulin (red) for the colocalization with NGFP-hCEP164-WT fusion proteins (green) (see also Figures 3B–3D). Scale bars, 10 μm. (G) Immunoblot of IMCD3 and hTERT-RPE cells expressing inducible GFP-CEP164 constructs confirmed doxycyclin-inducible NGFP-CEP164 fusion protein expression (~191 kDa) both with α-CEP164-NR and α-GFP antibody blotting (arrow heads). The band at ~85 kDa (asterisk) may represent the endogenous isoform 2 of CEP164 (84 kDa). IMCD3 and hTERT-RPE cells were stably transfected with the N terminally tagged-GFP-CEP164 construct in a retroviral vector (pRetroX-Tight-Pur) for doxycyclin-inducible expression. Cells were selected on puromycin for 2 weeks. Both cell lines were plated and treated with the indicated doses of doxycycline and lyzed with RIPA buffer 24 hr after induction. A total of 50 μg of cell lysates were loaded onto SDS-PAGE and blotted with the antibodies indicated. The same membranes were reprobed with anti-α-tubulin antibody as an indicator of equal loading (GFP-blotted membrane shown) (see also Figure 3). See also Figure 3.

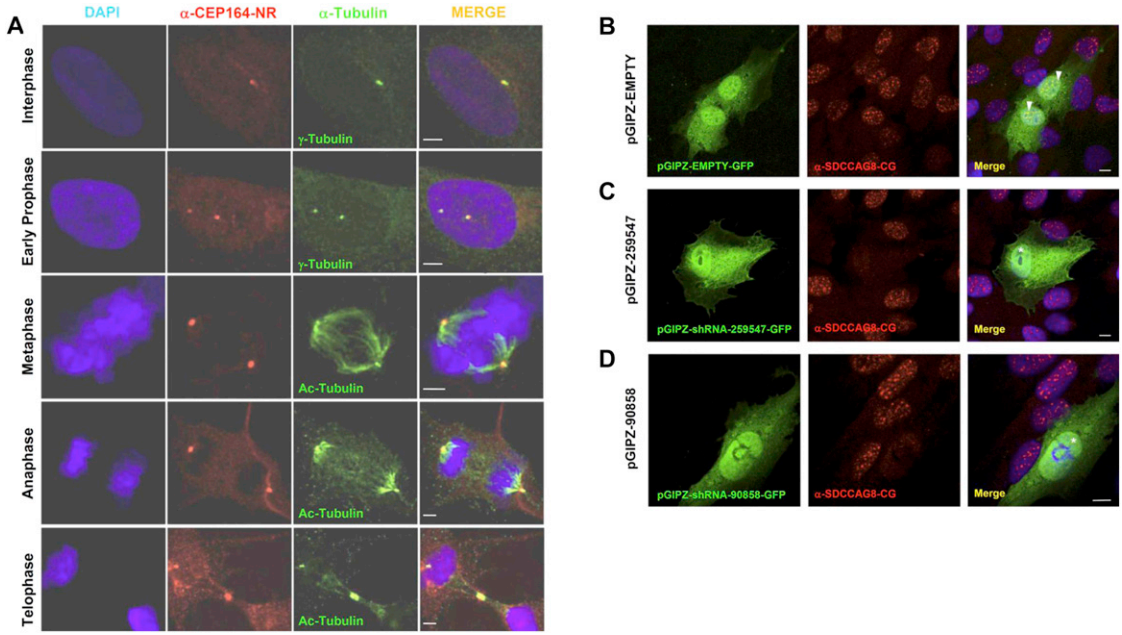

Figure S4. Subcellular Localization of CEP164 and SDCCAG8 by Immunofluorescence

(A) CEP164 colocalizes with the mother centriole (labeled with γ-tubulin), the mitotic spindle poles (actetylated tubulin), and the midbody throughout the cell cycle in hTERT-RPE cells. Whereas in the centriole-engaged state (upper panel) γ-tubulin antibody labels both centrioles, the α-CEP164 antibody only labels one centriole (the mother centriole) in hTERT cells. Immunofluorescence of endogenous CEP164 was performed in hTERT cells. Cells were fixed (4% PFA), permeabilized (0.1% SDS) and immuno-stained with antibody anti-CEP164-NR (red) and costained with anti-γ-tubulin or anti-acetylated tubulin antibodies (green). DAPI was used to label DNA (Blue). Scale bars, 2.5 μm.

(B)–(D) Upon immunofluorescence (IF) in hTERT-RPE cells antibody α-SDCCAG8-CG recognizes nuclear foci that are absent upon transient *SDCCAG8*/*NPHP10* knockdown. Left panels show transfected hTERT-RPE cells, middle panels show IF with α-SDCCAG8-CG, right panels show merge of left and middle panels. Antibody α-SDCCAG8-CG recognizes nuclear foci in hTERT-RPE cells (middle and right panels). (B) hTERT cells transiently transfected with GFP-labeled negative control shRNA construct exhibit nuclear foci upon IF with α-SDCCAG8-CG (arrow heads in right panel), whereas in cells transfected with GFP-labeled *SDCCAG8* shRNA knockdown constructs pGIPZ-259547 (C) or pGIPZ-90858 (D) nuclear foci are absent (asterisks in right panels of (C) and (D), demonstrating specificity of the nuclear foci signal detected by α-SDCCAG8-CG. Scale bars, 5 μm. See also Figure 4.

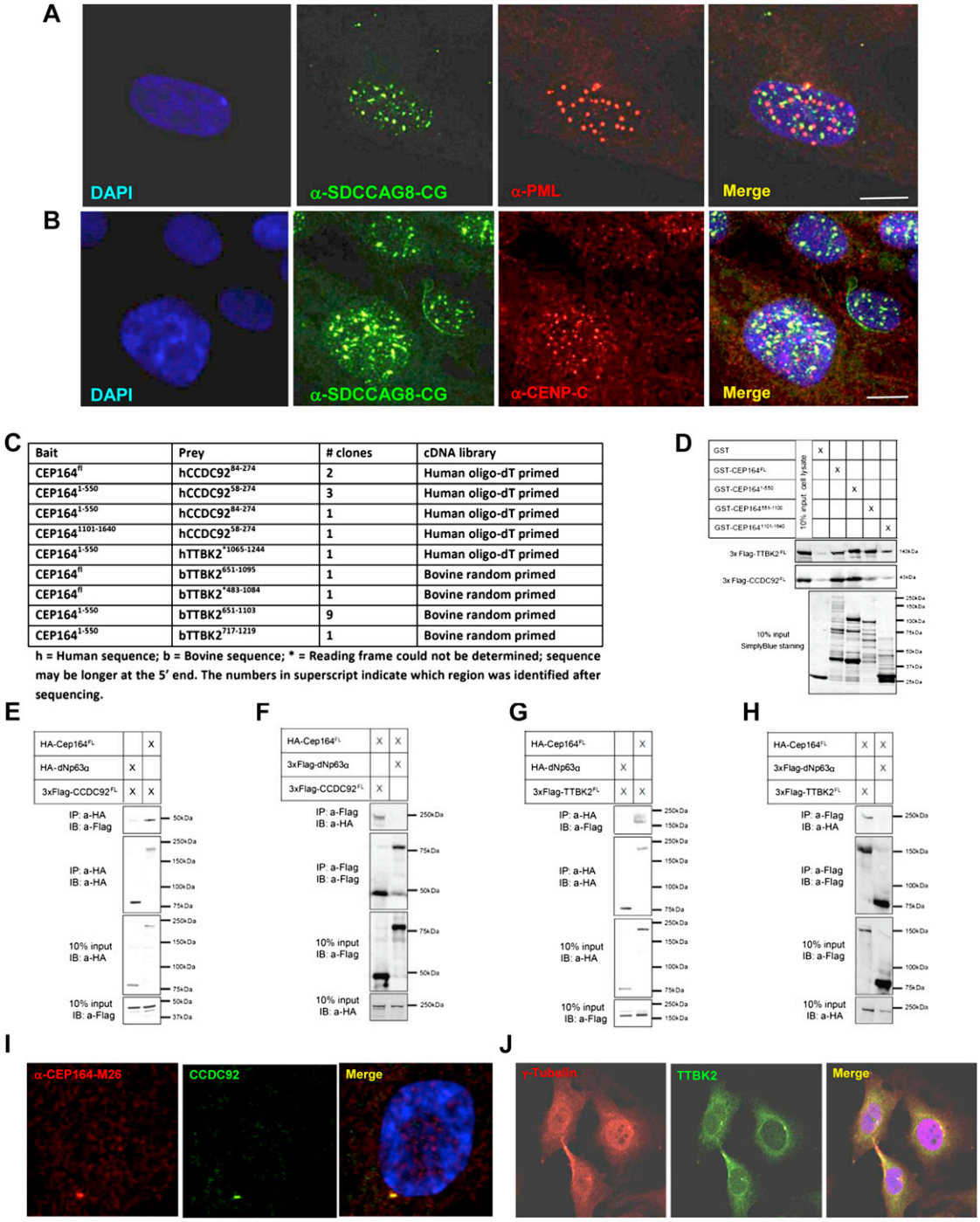

Bait	Prey	# clones	cDNA library
CEP164^{fl}	hCCDC92$^{84-274}$	2	Human oligo-dT primed
CEP164$^{1-550}$	hCCDC92$^{58-274}$	3	Human oligo-dT primed
CEP164$^{1-550}$	hCCDC92$^{84-274}$	1	Human oligo-dT primed
CEP164$^{1101-1640}$	hCCDC92$^{58-274}$	1	Human oligo-dT primed
CEP164$^{1-550}$	hTTBK2$^{*1065-1244}$	1	Human oligo-dT primed
CEP164^{fl}	bTTBK2$^{651-1095}$	1	Bovine random primed
CEP164^{fl}	bTTBK2$^{*483-1084}$	1	Bovine random primed
CEP164$^{1-550}$	bTTBK2$^{651-1103}$	9	Bovine random primed
CEP164$^{1-550}$	bTTBK2$^{717-1219}$	1	Bovine random primed

h = Human sequence; b = Bovine sequence; * = Reading frame could not be determined; sequence may be longer at the 5′ end. The numbers in superscript indicate which region was identified after sequencing.

Figure S5. (A–B) Immuofluorescence Imaging of the NPHP-RC Protein SDCCAG8/NPHP10 with Other Proteins of Nuclear Foci in hTERT-RPE Cells, and (C–J) Identification of CCDC92 and TTKB2 as Direct Interaction Partners of CEP164

(A–B) SDCCAG8 labeled with antibody α-SDCCAG8-CG exihibits a similar number and size of nuclear foci in comparison to signals from antibodies against the nuclear foci markers promyelocytic leukemia protein (PML) (A) and centromere protein C (CENP-C) (B). However, these proteins do not colocalize with SDCCAG8. Scale bars, 5 μm.

(C–J) Identification of CCDC92 and TTKB2 as direct interaction partners of CEP164. (C) Four baits, BD-CEP164^{fl}, BD-CEP164$^{1-550}$, BD-CEP164$^{551-1100}$, and BD-CEP164$^{1101-1640}$ were used to screen two retinal cDNA libraries, a human oligo-dT primed library and a bovine randomly primed library, employing a GAL-4 based yeast two-hybrid system. CEP164 was found to interact with two proteins, coiled coil domain containing protein 92 (CCDC92) and tau tubulin kinase 2 (TTBK2). The CEP164, CCDC92 and TTBK2 fragments are indicated with amino acids numbering in superscript. (D) Lysates from COS-1 cells transfected with 3xFlag-CCDC92^{fl} or 3xFlag-TTBK2^{fl} were used in a pull-down assay of GST fusion proteins GST-CEP164^{fl} (191kDa), GST-CEP$^{1-550}$ (87kDa), GST-CEP164$^{551-1100}$

(92kDa), and GST-CEP164$^{1101\text{-}1640}$ (68kDa). 3xFlag-CCDC92^{fl} preferentially binds GST-CEP164^{fl} and GST-CEP164$^{1\text{-}550}$, while 3xFlag-TTBK2^{fl} binds all four GST fusion proteins. The results are further confirmed by unbound GST (26kDa), which shows no interaction with 3xFlag-CCDC92^{fl} nor 3xFlag-TTBK2^{fl}. (E–F) For coimmunoprecipitation 3xHA-CEP164^{fl} in combination with 3xFlag-CCDC92^{fl} were overexpressed in COS-1 cells (10% protein input shown). In an anti-HA immunoprecipitation 3xHA-CEP164^{fl} coprecipitated with 3xFlag-CCDC92^{fl} (E), whereas the coprecipitation with the unrelated 3xHA-dNp63 is very limited. This was confirmed in the reciprocal coIP using an anti-Flag antibody against 3xFlag-CCDC92^{fl} (F).

(G–H) For coimmunoprecipitation 3xHA-CEP164^{fl} in combination with 3xFlag-TTBK2^{fl} were overexpressed in COS-1 cells (10% protein input shown). In an anti-HA immunoprecipitation of 3xHA-CEP164^{fl}, this protein coprecipitated with 3xFlag-TTBK2^{fl} (G), whereas the coprecipitation with the unrelated 3xHA-dNp63 was negative. This was confirmed in the reciprocal coIP using an anti-Flag antibody to immunoprecipitate 3xFlag-TTBK2^{fl} (H).

(I–J) (I) The α-CCDC92 antibody signal fully colocalizes with α-CEP164-M26 at the mother centriole upon immunofluorescence imaging in hTERT-RPE cells. (J) TTBK2 weakly colocalizes with α-CEP164-M26 at one of the centrioles, but yields a strong signal at the mid body in dividing hTERT-RPE cells. See also Figure 4.

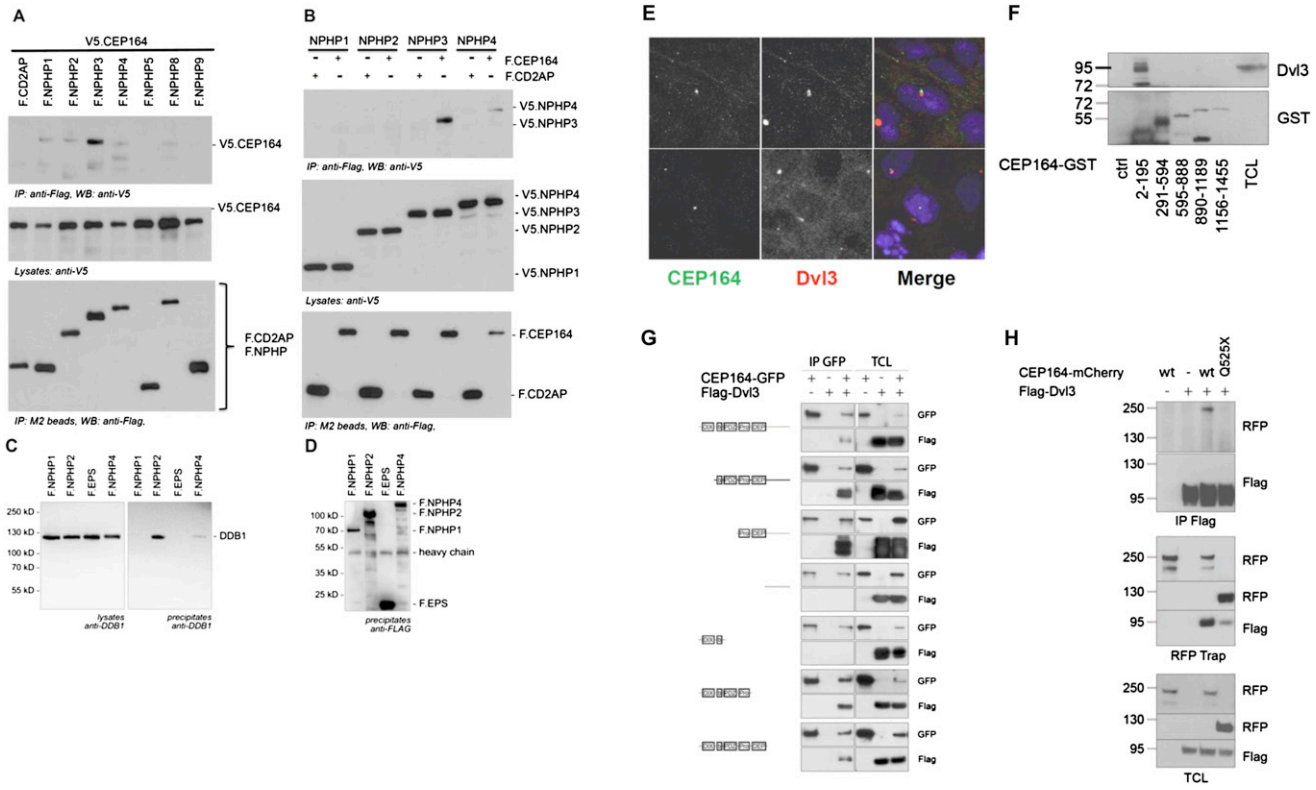

Figure S6. Molecular Interaction of NPHP-RC Gene Products with DDR Proteins.

(A and B) Interaction of NPHP3 with CEP164. (A) To determine whether CEP164 interacts with known NPHP proteins, HEK293T cells were cotransfected with expression constructs for N terminally V5-tagged human full-length CEP164 and FLAG-tagged human full length NPHP1-NPHP5, NPHP8, NPHP9, or the control protein CD2AP as indicated. Comparable amounts of CEP164 were present in all lysates (middle panel). NPHP proteins were precipitated, using anti-Flag M2 beads (bottom panel). NPHP3 immobilized V5-tagged CEP164; a weak interaction was also detectable for NPHP1, 2 and 4 (top panel). (B) The reciprocal interaction confirmed an interaction between CEP164 and NPHP3. Flag-tagged CEP164 or CD2AP were coexpressed with V5-tagged NPHP1-NPHP4. Precipitation of NPHP3, but not the control protein CD2AP immobilized V5-tagged NPHP3. A weak, but reproducible interaction was also detected for NPHP4 (top panel).

(C and D) Interaction of NPHP2 with DDB1. (C) HEK293T cells were transiently transfected with the Flag-tagged NPH-proteins NPHP1, NPHP2, NPHP4 or a control protein (Flag-EPS). Following immunoprecipitation with Flag-antibody Western blot analysis revealed that endogenous DDB1 coprecipitated with NPHP2 and to a lesser extent with NPHP4 but not with NPHP1 or the control protein.

(D) Control experiment for protein expression using anti-FLAG antibody.

(E and H) Cep164 and Dvl3 are in a precipitable complex. (E) CEP164 and Dvl colocalize at centrosomes. Whereas CEP164 is known to localize to the mother centriole only, Dvl3 is noted to label both centrioles (upper panel) or to the daughter centriole only (lower panel). HEK293 cells were fixed, labeled with antibody α-CEP164-PR and α-Dvl3. (F) Domain mapping of the CEP164 interaction with Dvl3. Series of bacterially produced CEP164-GST fragments were incubated with HEK293 cell lysates, precipitated using GST pull-down, and probed for presence of Dvl3 by immunoblotting against Dvl3 and GST, respectively. Endogenous Dvl3 interacts with a region within the first 194 amino acids of CEP164, which corresponds to the ATRIP binding domain. (G) CEP164 interacts with the proline-rich region of Dvl3. HEK293 cells were transfected with GFP-tagged full-length human CEP164 and a panel of truncation mutants of Flag-Dvl3 as indicated, and coimmunoprecipitation was performed with an anti-GFP antibody. Note that CEP164 only interacts with Dvl3 fragments that contain the proline-rich region (Pro). (H) Full length CEP164 but not the mutant CEP164-Q525X interacts with Dvl3. HEK293 cells were transfected with the indicated plasmids and subjected to immunoprecipitation using antibodies against FLAG-Dvl3 (upper panel) or CEP164-mCherryRFP (middle panel). Immunoblot analysis demonstrates strong interaction with Dvl3 for wild-type (wt) CEP164-mCherryRFP, whereas interactions is strongly reduced for CEP164-Q525X to Dvl3.

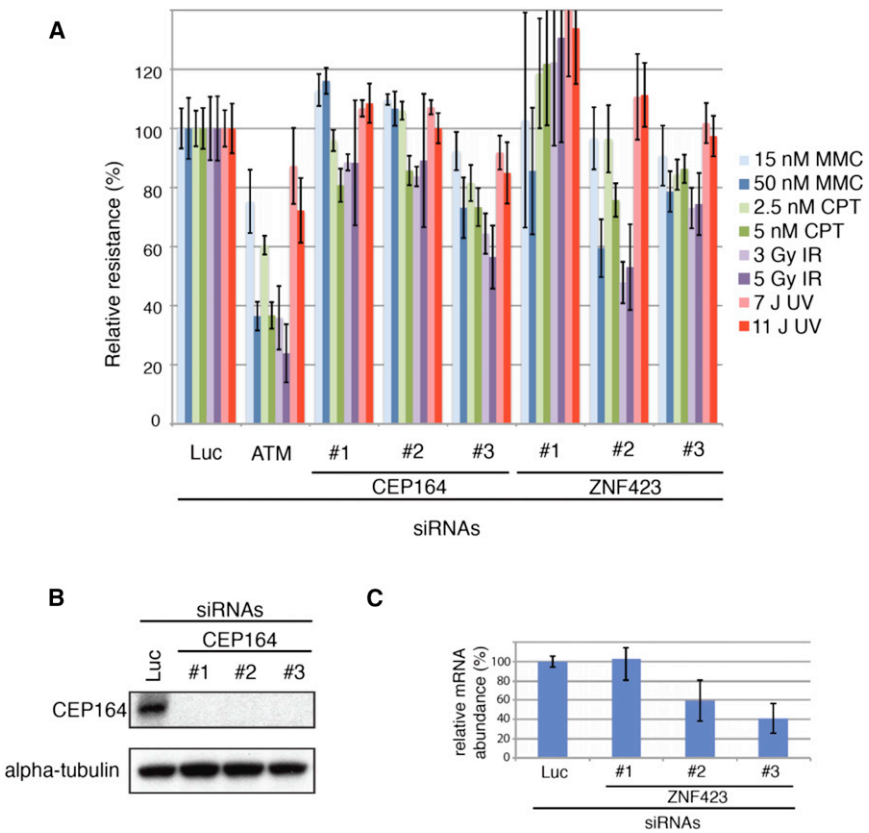

Figure S7. Depletion of *CEP164* or *ZNF423(Zpf423)* Results in Sensitivity to DNA Damaging Agents

(A) Multicolor competition assay (MCA) (Smogorzewska et al., 2007). GFP-U2OS cells were transfected with the indicated siRNAs against *CEP164* and *ZNF423*. Seventy-two hours after after transfection they were mixed with RFP-U2OS cells transfected with Luciferase (Luc) and DNA damage was induced using the indicated agents. After 7 days, percent of gfp-positive cells was measured using fluorescence-activated cell sorting and the resistance to DNA damage was calculated in comparison to untreated cells. DNA damage resistance was set at 100% for GFP-U2OS cells transfected with an siRNA against Luciferase (Luc). Cells transfected with siRNAs against *ATM* were used as a positive control. Experiments were done in triplicate. Standard deviations are indicated.

Depletion of *CEP164* (B) led to sensitivity to camptothecin (CPT) and gamma irradiation (IR). In addition, depletion with siRNA #3 led to sensitivity to mitomycin C (MMC). Furthermore, transfection of two separate *ZNF423* siRNAs (#2 and #3), that resulted in *ZNF423* mRNA depletion as assessed by RT-qPCR (C), caused sensitivity to MMC, CPT, and IR (L). An siRNA that did not result in *ZNF423* mRNA depletion (C), siRNA #1 did not result in increased sensitivity to DNA damage.

(B) Western blot analysis of *CEP164* expression after siRNA transfection in cells used in the MCA assay shown in (A)

(C) RT-qPCR in U2OS cells transfected with the three siRNAs against *ZNF423* used in the MCA assay shown in (A). Reactions were performed in triplicate. Standard deviations are indicated.

See also Figure 6.